

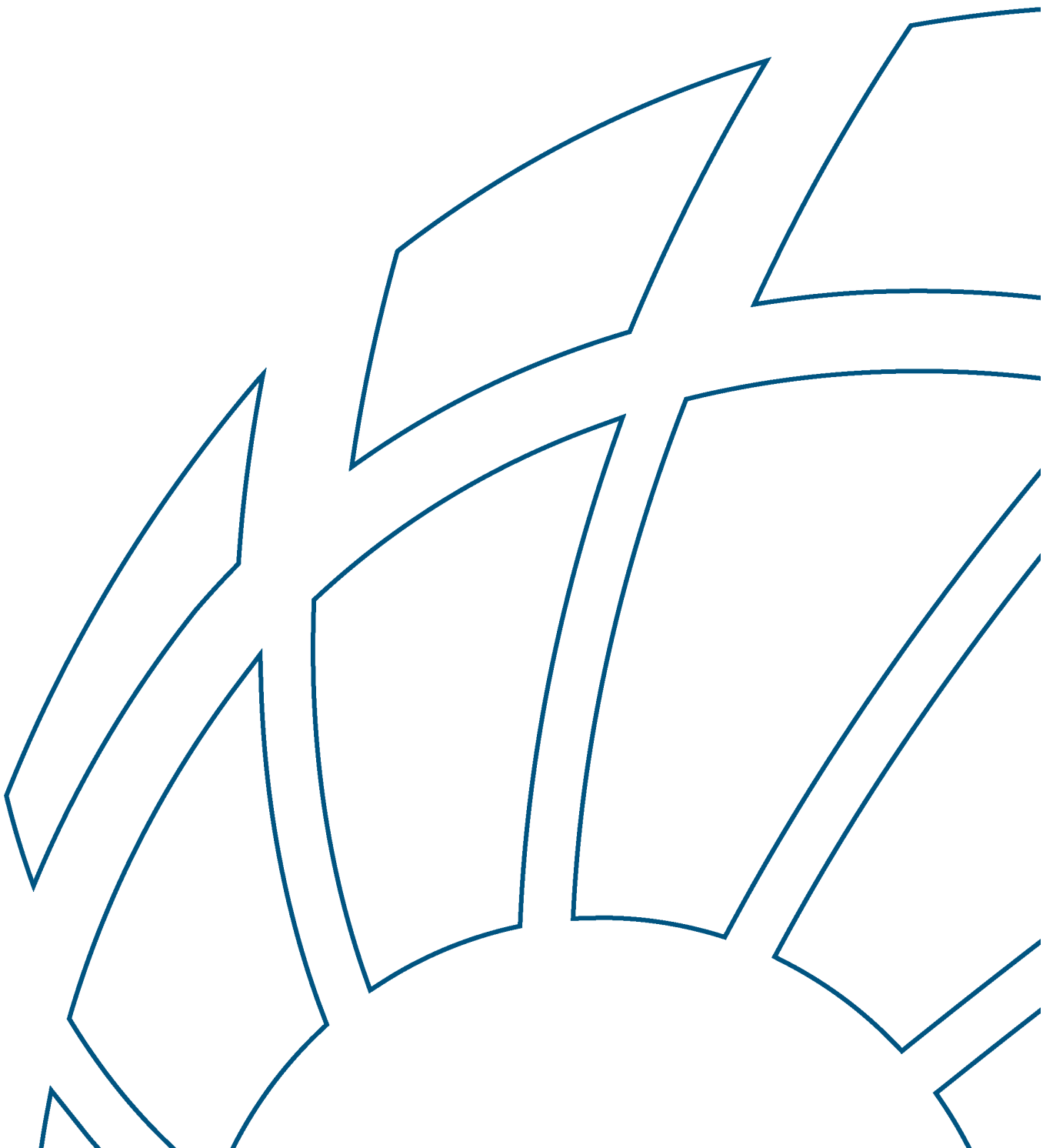


Perth Desalination Plant Discharge Modelling: Model Validation

Reference: R.B22253.002.04.ModelValidation_PRP.docx

Date: August 2018



Confidential



Document Control Sheet

<p>BMT Eastern Australia Pty Ltd Level 8, 200 Creek Street Brisbane Qld 4000 Australia PO Box 203, Spring Hill 4004</p> <p>Tel: +61 7 3831 6744 Fax: + 61 7 3832 3627</p> <p>ABN 54 010 830 421</p> <p>www.bmt.org</p>	Document:	R.B22253.002.04.ModelValidation_PRP.d OCX
	Title:	Perth Desalination Plant Discharge Modelling: Model Validation
	Project Manager:	Michael Barry, Daniel Botelho
	Authors:	Daniel Botelho, Stephanie Lyons, Louise Bruce, Aditya Singh, Michael Barry
	Client:	Water Corporation
	Client Contact:	Ben Boardman
	Client Reference:	-
Synopsis: This report details development and calibration of the near and farfield models of the Perth Desalination Plant discharge into Cockburn Sound.		

REVISION/CHECKING HISTORY

Revision Number	Date	Checked by		Issued by	
0	27 th July 2017			DAB	
1	9 th October 2017	MEB		DAB	
2	6 th November 2017	MEB		DAB	
3	8 th August 2018	MEB		DAB	
4	9 th August 2018	MEB		DAB	

DISTRIBUTION

Destination	Revision										
	0	1	2	3	4	5	6	7	8	9	10
Water Corporation	Word	PDF	PDF	PDF	PDF						
BMT File		PDF	PDF	PDF	PDF						
BMT Library		PDF	PDF	PDF	PDF						

Copyright and non-disclosure notice

The contents and layout of this report are subject to copyright owned by BMT Eastern Australia Pty Ltd (BMT EA) save to the extent that copyright has been legally assigned by us to another party or is used by BMT EA under licence. To the extent that we own the copyright in this report, it may not be copied or used without our prior written agreement for any purpose other than the purpose indicated in this report.

The methodology (if any) contained in this report is provided to you in confidence and must not be disclosed or copied to third parties without the prior written agreement of BMT EA. Disclosure of that information may constitute an actionable breach of confidence or may otherwise prejudice our commercial interests. Any third party who obtains access to this report by any means will, in any event, be subject to the Third Party Disclaimer set out below.

Third Party Disclaimer

Any disclosure of this report to a third party is subject to this disclaimer. The report was prepared by BMT EA at the instruction of, and for use by, our client named on this Document Control Sheet. It does not in any way constitute advice to any third party who is able to access it by any means. BMT EA excludes to the fullest extent lawfully permitted all liability whatsoever for any loss or damage howsoever arising from reliance on the contents of this report.

Executive Summary

Executive Summary

This report describes the construction and validation of a three-dimensional hydrodynamic, transport and dissolved oxygen (DO) model of Cockburn Sound and its surrounds, Western Australia (the farfield model). The existing PSDP discharge plume was also represented by constructing and dynamically linking a high-resolution three dimensional nearfield model of the PSDP diffuser to the farfield model. The PSDP discharge was included in model construction because it has existed since 2007 and plays a role in modifying natural processes. It was not included for impact assessment purposes, although doing so may form part of future deployments of the Cockburn Sound modelling suite developed as part of this study.

The farfield model was validated against a range of data sets that included water levels, velocities, temperature, salinity and DO measurements, and over a number of separate periods. Validation of the nearfield model was made against literature values and nearfield measurements undertaken by others. The model was also validated in the intermediate field, where the PSDP plume transitioned from the confinement of a navigation channels to the Sound's deep basin.

A series of animations of model predictions have been prepared and form part of this report. They can be shared by BMT on request from Water Corporation.

List of Abbreviations

List of Abbreviations

ADCP – Acoustic-Doppler Current Profiler

AED2 – Aquatic Ecosystem Model v.2

AMC - Australian Marine Complex

AHD – Australian Height Datum

ANZECC - Australian and New Zealand Environment and Conservation Council

ARMCANZ - Agriculture and Resources Management Council of Australia and New Zealand

BMT – British Maritime Technology

BoM – Bureau of Meteorology

CD – Chart Datum

CFD – Computational Fluid Dynamics

CFSv2 – Climate Forecast System version 2

CKB – Cockburn Power Station

CSMC - Cockburn Sound Management Council

CSW – Coastal Shelf Waves

CWR – Centre for Water Research

DEM – Digital Elevation Model

DEP – Department of Environmental Protection

DO – Dissolved Oxygen

DoT - Department of Transport

ELCOM – Estuary Lake and Coastal Ocean Model

FPA - Fremantle Ports Authority

GA – Geosciences Australia

GEBCO - General Bathymetric Chart of the Oceans

GL - Gigalitre

GOTM – General Ocean Turbulence Model

HARC – Hydrology and Risk Assessment

HPC – High Performance Computing

HYCOM – HYbrid Coordinate Ocean Model

IOA – Index of Agreement

KIA – Kwinana Industrial Area

List of Abbreviations

KPS – Kwinana Power Station

KPS-C – Kwinana Power Station Stage C

KPS-GF – Kwinana Power Station Gas Fired

LAT – Lowest Astronomic Tide

LWMF – Low Water Mark at Fremantle

MAE – Mean Absolute Error

MAFRL - Marine and Freshwater Research Laboratory

MMMP – Marine Monitoring and Management Plan

NCEP – National Center for Environmental Prediction

NCODA – Navy Coupled Ocean Data Assimilation System

NLSWE – Nonlinear Shallow Water Equations

OEPA - Office of the Environmental Protection Authority

OpenFOAM - Open Field Operation and Manipulation

PSDP – Perth Seawater Desalination Plant

RAAF - Royal Australian Air Force

RMSE – Root Mean Square Error

RTMS – Real Time Monitoring System

RWT - Rhodamine WT

SOD – Sediment Oxygen Demand

SEP – State Environmental (Cockburn Sound) 2005 Policy

TC – Tropical Cyclones

UNESCO – United Nations Educational, Scientific and Cultural Organization

Contents

Contents

Executive Summary	i
List of Abbreviations	ii
1 Introduction	1
1.1 Background	1
1.2 Scope of this report	1
2 Site characterisation	2
2.1 Setting and morphology	2
2.2 Meteorology and hydrodynamics	5
2.2.1 Climate drivers	5
2.2.1.1 General	5
2.2.1.2 Summer to Early Autumn Climate	5
2.2.1.3 Autumn to Early Spring Climate	12
2.2.2 Hydrodynamics	18
2.2.2.1 Wind-driven currents	18
2.2.2.2 Density gradients	23
2.2.2.3 Continental shelf waves	24
2.2.2.4 Secondary influences	26
2.3 Dissolved oxygen	27
2.3.1 Low DO events	31
2.4 PSDP discharge characteristics	37
2.4.1 Plume mixing and behaviour	40
2.5 Summary	43
3 Nearfield model	44
3.1 Model package	44
3.2 CFD model setup	45
3.2.1 Equations	45
3.2.2 Turbulence model	46
3.2.3 Domain and mesh	46
3.2.4 Boundary conditions	48
3.2.4.1 Ambient currents and outfall discharge	49
3.3 Model results	49
3.3.1 Dilutions in the nearfield	53
4 Farfield model	54

Contents

4.1	Water quality model (AED2)	54
4.2	Hydrodynamic model (TUFLOW FV)	55
4.3	Model domain, mesh and bathymetry	55
4.4	Boundary conditions	59
4.4.1	Wind	59
4.4.2	Tides	60
4.4.3	Regional currents, salinity, temperature, and DO	60
4.4.4	Radiation, precipitation and humidity	64
4.4.5	Air temperature	64
4.4.6	Swan River flows	64
4.4.7	PSDP discharge	65
4.4.7.1	Modelling approach	65
4.4.7.2	Linkage technique	66
4.4.7.3	Model integration	66
4.4.7.4	Salinity, temperature and DO	67
4.4.8	Intakes and other discharges	67
4.5	Turbulence closure scheme	70
4.6	Hydrodynamic model parameterisation	70
5	Model simulations	71
5.1	Water level comparisons	72
5.1.1	Measurement specifications	72
5.1.2	Model Comparisons	72
5.2	Velocity comparisons	80
5.2.1	Measurement specifications	80
5.2.2	Model comparisons	80
5.2.2.1	May to July 2006	80
5.2.2.2	January to March 2007	90
5.3	Temperature and salinity comparisons	98
5.3.1	Measurement specifications	98
5.3.1.1	Deep basin	98
5.3.1.2	MMMP array	101
5.3.2	Model comparisons (2008)	101
5.3.2.1	Summer to early autumn 2008 - temperatures	101
5.3.2.2	Summer to early autumn 2008 - salinities	109
5.3.2.3	Winter to spring 2008 - temperatures	112
5.3.2.4	Winter to spring 2008 – salinities	116
5.3.2.5	Model Error	120

Contents

5.3.3	Stratification duration	124
5.3.4	PSDP discharge plume	128
5.3.4.1	Transect 1: 0800 hrs	129
5.3.4.2	Transect 2: 1100 hrs	131
5.3.4.3	Transect 3: 1300 hrs	133
5.3.4.4	Transect 3: 1500 hrs	135
5.3.4.5	Transect 3: 1600 hrs	137
5.3.4.6	Transect 3: 1700 hrs	139
5.3.5	Model comparisons (2013)	141
5.3.5.1	Continuous temperature measurements	141
5.3.5.2	Temperature and salinity profiles in the deep basin	143
5.3.5.3	Temperature and salinity profiles in the transition to the deep basin	143
5.3.6	Model Comparisons (2011)	160
5.3.6.1	Temperature and salinity profiles in the deep basin	160
5.3.6.2	Temperature and salinity profiles in the transition to the deep basin	162
5.4	Evaporation Rates	165
5.5	DO comparisons	165
5.5.1	Water quality model parameterisation	165
5.5.2	Summer to early autumn 2008	168
5.5.2.1	Sediment oxygen demand	174
5.5.3	Winter to spring 2008	174
5.5.3.1	Sediment oxygen demand	179
5.5.4	Model error	179
5.5.5	Summer to early autumn 2013	182
5.5.5.1	DO profiles in the deep basin	182
5.5.5.2	DO profiles in the transition to the deep basin	182
5.5.5.3	Data mapping	190
5.5.6	March 2011	229
5.5.6.1	DO profiles in the deep basin	229
5.5.6.2	DO profiles in the transition to the deep basin	230
5.6	Fish kill event (November 2015)	232
5.6.1	Event	232
5.6.2	Prevailing synoptic patterns	233
5.6.3	Hydrodynamic state	233
5.6.4	Simulation	233
5.6.5	Predicted temporal Patterns	235
5.6.5.1	Evolution of temperature, salinity and DO profiles	235

Contents

5.6.5.2	Near-surface to near-bed differences	239
5.6.5.3	Spatial patterns	241
6	Discussion and Summary	273
6.1	Nearfield CFD Modelling	273
6.2	Farfield Modelling	273
6.2.1	Model performance	274
6.2.2	Fish kill event	275
6.2.3	Summary	275
7	References	276
Appendix A	Additional iso-dilution surfaces from the CFD simulations	A-1
Appendix B	Hydraulic model of the Swan River	B-1
Appendix C	Linkage technique details	C-1
Appendix D	Statistics for model validation	D-1
Appendix E	Comparisons between model and ADCP measurements	E-1
Appendix F	Bottom roughness sensitivity analysis	F-1
Appendix G	RTMS data temperature comparisons	G-1
Appendix H	Animations	H-1
Appendix I	Model error for scalars	I-1
Appendix J	Temperature, salinity and DO comparisons in March 2011	J-1
Appendix K	Horizontal salinity contour maps	K-1

List of Figures

Figure 2-1	Perth Seawater Desalination Plant and outfall locality	3
Figure 2-2	Digital elevation model of Cockburn Sound and Surrounds	4
Figure 2-3	Sequence of synoptic weather charts between 28 February and 11 March 2008 (Panels A to L). Same period as in Figure 2-5. Graphs accessed from the BoM web site.	8
Figure 2-4	Meteorological and sampling stations in Cockburn Sound	10
Figure 2-5	Wind and Air temperature at Garden Island: 28 February and 11 March 2008	11
Figure 2-6	Sequence of synoptic weather charts between 21 July and 05 August 2008 (Panels A to O). Same period in Figure 2-7. Graphs accessed from the BoM web site.	14
Figure 2-7	Wind, Air temperature and Rainfall at Garden Island: 21 July to 05 August 2008	17
Figure 2-8	Wind field (BoM station at Gardens Island) and currents (FPA data) in Cockburn Sound from 18 and 30 June 2006. Left panels: Spoil Grounds	

Contents

	station. Right Panel: Northern Basin station. Wind data is the same on both left and right panels.	21
Figure 2-9	Wind field (BoM station at Gardens Island) and currents (FPA data) in Cockburn Sound from 24 March to 03 March 2007. Left panels: Spoil Grounds station. Right Panel: Northern Basin station. Wind data is the same on both left and right panels.	22
Figure 2-10	The annual cycle in the salinity and temperature differences (ΔS and ΔT , respectively) between Central Cockburn Sound and the mid shelf at 10 m depth (from D'Adamo, 2002)	23
Figure 2-11	Tidal records at Mangles Bay from 12 January to 30 April 2007. Upper panel: Raw tidal record. Middle panel: harmonic components. Lower panel: residual water levels.	26
Figure 2-12	Dissolved oxygen, density, temperature and salinity measurements in Cockburn Sound	30
Figure 2-13	Tidal records at Mangles Bay from 15 February to 15 March 2008. Upper panel: Raw tidal record. Middle panel: harmonic components. Lower panel: residual water levels.	31
Figure 2-14	Continuous DO Monitoring conducted by the Water Corporation as part of the MMMP (Water Corporation 2013)	32
Figure 2-15	Wind speed and DO saturation during the low DO events of 2011 and 2013 (Water Corporation 2013)	32
Figure 2-16	Locations at which profile data were sampled as part of the MMMP in April 2013 (from Water Corporation 2013)	34
Figure 2-17	Dissolved oxygen, density, temperature and salinity measurements in Cockburn Sound in April 2013	35
Figure 2-18	Dissolved oxygen, density, temperature and salinity measurements near Stirling channel entry in Cockburn Sound in April 2013. South Buoy profiles are also plotted for reference.	36
Figure 2-19	Seawater intake and outfall general arrangement	38
Figure 2-20	Seawater intake & outfall – double tee diffuser arrangement GA & section	39
Figure 2-21	Definition diagram for nearfield characteristics (adapted from Roberts et al. 1997)	40
Figure 2-22	Ensemble average of saline discharge layer height (top panel) and dilution (bottom panel) for bins corresponding to 5 m intervals away from diffuser for full flow. Horizontal line in background of top panel show theoretical layer thickness from Roberts et al. (1997). Symbols in bottom panel show location and dilution at impact point (circle) and edge of mixing zone (square) predicted by Roberts et al. (1997). The horizontal line on the bottom panel represents the design target dilution of 45 times (marked from 50 metres from the diffuser onwards). (reproduced from CWR 2007a)	41
Figure 2-23	Measured (upper panel) and simulated (lower panel) salinity along a transect from the diffuser to the main shipping channel following the dye release in the morning of 26 Apr 2007. Locations of transect profiles are shown on the map	

Contents

	to the right of each panel; map has diffuser marked; red symbols indicate profile closest to diffuser. (Reproduced from CWR 2007).	42
Figure 2-24	Transect of measured (upper panel) and simulated (lower panel) salinity along the main shipping channel and off the shelf during the middle of the day on 26 Apr 2007, 2-5 hours after the dye release (Reproduced from CWR 2007).	42
Figure 3-1	Surface mesh showing resolution increase towards the diffuser ports	47
Figure 3-2	Surface mesh at the diffuser ports	47
Figure 3-3	Adaptive mesh refinement	48
Figure 3-4	Effluent plume resulting from CFD simulations. Results depict the 1:20 iso-surface dilution	51
Figure 3-5	Definition diagram for nearfield characteristics (reproduced from Roberts et al. 1997)	52
Figure 3-6	Cross-section illustrating brine concentration field for comparisons with Roberts and Abessi (2014) scaling	52
Figure 4-1	AED2 dissolved oxygen governing equations	55
Figure 4-2	Hydrodynamic model extent and bathymetry	57
Figure 4-3	Hydrodynamic model mesh detail	58
Figure 4-4	Comparison between Garden Island and CFSv2 wind data at nearest grid location	60
Figure 4-5	Locations where CFSv2 data were available	61
Figure 4-6	Locations where TOPEX data were available	62
Figure 4-7	Locations where HYCOM + NCODA data were available	63
Figure 4-8	Swan River Flows	64
Figure 4-9	Temperature and Salinity Specification at Swan River Mouth	65
Figure 4-10	Schematic of the translation of the nearfield effluent mass distribution into the farfield Model	67
Figure 5-1	Comparison between measured and simulated water levels at Mangles Bay for May to July 2006	74
Figure 5-2	Comparison between measured and simulated water levels at Mangles Bay for January to March 2007	75
Figure 5-3	Comparison between measured and simulated water levels at Mangles Bay for January to April 2008	76
Figure 5-4	Comparison between measured and simulated water levels at Mangles Bay for March 2011	77
Figure 5-5	Comparison between measured and simulated water levels at Stirling Channel Beacon 5 for April 2013	78
Figure 5-6	Comparison between measured and simulated water levels at Stirling Channel Beacon 5 for October to November 2015	79
Figure 5-7	Comparisons between simulated velocities and ADCP measurements at Spoil Grounds for May to July 2006	83

Contents

Figure 5-8	Comparison between simulated and measured ADCP velocities at 5.1m from sea bed at Spoil Grounds for May to July 2006	84
Figure 5-9	Comparison between simulated and measured ADCP velocities at 3.6m from sea bed at Spoil Grounds for May to July 2006	84
Figure 5-10	Comparison between simulated and measured ADCP velocities at 1.6m from sea bed at Spoil Grounds for May to July 2006	84
Figure 5-11	Comparisons between simulated velocities and ADCP measurements at Northern Basin for May to July 2006	85
Figure 5-12	Comparison between simulated and measured ADCP velocities at 15.5m from the sea bed at Northern Basin for May to July 2006	86
Figure 5-13	Comparison between simulated and measured ADCP velocities at 9.5m from the sea bed at Northern Basin for May to July 2006	86
Figure 5-14	Comparison between simulated and measured ADCP velocities at 2.5m from the sea bed at Northern Basin for May to July 2006	86
Figure 5-15	Response to field data and simulation results to a wind shifting from north to south-east (28 to 30 May 2006)	87
Figure 5-16	Response to field data and simulation results to a wind shifting from north to south-east (14 to 16 May 2006)	88
Figure 5-17	Comparisons between simulated velocities and ADCP measurements at Spoil Grounds for February to March 2007	91
Figure 5-18	Comparison between simulated and measured ADCP velocities at 5.1m from sea bed at Spoil Grounds for February to March 2007	92
Figure 5-19	Comparison between simulated and measured ADCP velocities at 3.6m from sea bed at Spoil Grounds for February to March 2007	92
Figure 5-20	Comparison between simulated and measured ADCP velocities at 1.6m from sea bed at Spoil Grounds for February to March 2007	92
Figure 5-21	Response to field data and simulation results to different wind regimes at Spoil Grounds (27 February to 11 March 2007)	93
Figure 5-22	Comparisons between simulated velocities and ADCP measurements at Northern Basin for February to March 2007	94
Figure 5-23	Comparison between simulated and measured ADCP velocities at 5.1m from sea bed at Northern Basin for February to March 2007	95
Figure 5-24	Comparison between simulated and measured ADCP velocities at 3.6m from sea bed at Northern Basin for February to March 2007	95
Figure 5-25	Comparison between simulated and measured ADCP velocities at 1.6m from sea bed at Northern Basin for February to March 2007	95
Figure 5-26	Response to field data and simulation results to different wind regimes at Northern Basin (27 February to 11 March 2007)	96
Figure 5-27	Salinity comparison between RTMS (lines) and profile data (points) at North Buoy from January to March 2008	99
Figure 5-28	Salinity comparison between RTMS (lines) and profile data (points) at North Buoy from August to October 2008	99

Contents

Figure 5-29	Salinity comparison between RTMS (lines) and profile data (points) at Central Buoy from January to March 2008	100
Figure 5-30	Salinity comparison between RTMS (lines) and profile data (points) at Central Buoy from August to October 2008	100
Figure 5-31	Salinity comparison between RTMS (lines) and profile data (points) at South Buoy from January to March 2008	101
Figure 5-32	Salinity comparison between RTMS (lines) and profile data (points) at South Buoy from August to October 2008	101
Figure 5-33	Comparisons between simulated temperatures and RTMS measurements at North Buoy in summer 2008	104
Figure 5-34	Comparisons between simulated temperatures and profile measurements at North Buoy in summer 2008	104
Figure 5-35	Comparisons between simulated temperatures and RTMS measurements at Central Buoy in summer 2008	105
Figure 5-36	Comparisons between simulated temperatures and profile measurements at Central Buoy in summer 2008	105
Figure 5-37	Comparisons between simulated temperatures and RTMS measurements at South Buoy in summer 2008	106
Figure 5-38	Comparisons between simulated temperatures and profile measurements at South Buoy in summer 2008	106
Figure 5-39	Wind and air temperature from BoM station at Garden Island (16 to 28 February 2008)	107
Figure 5-40	Wind and air temperature from BoM station at Garden Island (28 February to 11 March 2008)	108
Figure 5-41	Comparisons between simulated salinities and profile measurements at North Buoy in the transition from summer to autumn 2008	110
Figure 5-42	Comparisons between simulated salinities and profile measurements at Central Buoy in the transition from summer to autumn 2008	110
Figure 5-43	Comparisons between simulated salinities and profile measurements at South Buoy in the transition from summer to autumn 2008	111
Figure 5-44	Comparisons between simulated temperatures and RTMS measurements at North Buoy in in the transition from winter to spring 2008	113
Figure 5-45	Comparisons between simulated temperatures and profile measurements at North Buoy in in the transition from winter to spring 2008. Note: profiles measured on 16 and 30 October were considered inaccurate (see text).	113
Figure 5-46	Comparisons between simulated temperatures and RTMS measurements at Central Buoy in in the transition from winter to spring 2008	114
Figure 5-47	Comparisons between simulated temperatures and profile measurements at Central Buoy in in the transition from winter to spring 2008. Note: profiles measured on 16 and 30 October were considered inaccurate (see text).	114
Figure 5-48	Comparisons between simulated temperatures and RTMS measurements at South Buoy in in the transition from winter to spring 2008	115

Contents

Figure 5-49	Comparisons between simulated temperatures and profile measurements at South Buoy in the transition from winter to spring 2008	115
Figure 5-50	Comparisons between simulated salinities and profile measurements at North Buoy in the transition from winter to spring 2008	117
Figure 5-51	Comparisons between simulated salinities and profile measurements at Central Buoy in the transition from winter to spring 2008	117
Figure 5-52	Comparisons between simulated salinities and profile measurements at South Buoy in the transition from winter to spring 2008	117
Figure 5-53	Swan River plume interacting with Cockburn Sound – 1 of 6	118
Figure 5-54	Swan River plume interacting with Cockburn Sound – 2 of 6	118
Figure 5-55	Swan River plume interacting with Cockburn Sound – 3 of 6	118
Figure 5-56	Swan River plume interacting with Cockburn Sound – 4 of 6	119
Figure 5-57	Swan River plume interacting with Cockburn Sound – 5 of 6	119
Figure 5-57	Swan River plume interacting with Cockburn Sound – 6 of 6	119
Figure 5-58	Model predictive skill statistics for temperature and salinity profiles at North Buoy (top and bottom values)	123
Figure 5-59	Model predictive skill statistics for temperature and salinity profiles at Central Buoy (top and bottom values)	123
Figure 5-60	Model predictive skill statistics for temperature and salinity profiles at South Buoy (top and bottom values)	123
Figure 5-61	Temperature, salinity and density stratification in the transition from summer to autumn 2008 at North Buoy.	125
Figure 5-62	Temperature, salinity and density stratification in the transition from summer to autumn 2008 at Central Buoy.	125
Figure 5-63	Temperature, salinity and density stratification in the transition from summer to autumn 2008 at South Buoy.	126
Figure 5-64	Temperature, salinity and density stratification in the transition from winter to spring 2008 at North Buoy.	126
Figure 5-65	Temperature, salinity and density stratification in the transition from winter to spring 2008 at Central Buoy.	127
Figure 5-66	Temperature, salinity and density stratification in the transition from winter to spring 2008 at South Buoy.	127
Figure 5-67	Comparison of the wind patterns between Mar 2008 and Apr 2007. Vertical red lines delineate approximate sample or model extraction times	128
Figure 5-68	Comparison of the salinity profiles along the main shipping channel. The difference in background salinity predicted by the BMT model is a result of the different month of the year it considers, compared to the CWR (2007) measurements	130
Figure 5-69	Comparison of the salinity profiles along a transect from the diffuser to the main shipping channel. The difference in background salinity predicted by the BMT model is a result of the different month of the year it considers, compared to the CWR (2007) measurements	132

Contents

Figure 5-70	Comparison of the salinity profiles along the main shipping channel and off the shelf. The difference in background salinity predicted by the BMT model is a result of the different month of the year it considers, compared to the CWR (2007) measurements	134
Figure 5-71	Comparison of the salinity profiles along a section of the main shipping channel and near the diffuser. The difference in background salinity predicted by the BMT model is a result of the different month of the year it considers, compared to the CWR (2007) measurements	136
Figure 5-72	Comparison of the salinity profiles along the main shipping channel north of the diffuser. The difference in background salinity predicted by the BMT model is a result of the different month of the year it considers, compared to the CWR (2007) measurements	138
Figure 5-73	Comparison of the salinity profiles along the main shipping channel and embayment north of the diffuser. The difference in background salinity predicted by the BMT model is a result of the different month of the year it considers, compared to the CWR (2007) measurements	140
Figure 5-74	Measured (top) and simulated (bottom) water temperature data at the Central Buoy station. Horizontal black line indicates limit of top-most RTMS measurement	142
Figure 5-75	Measured (top) and simulated (bottom) water temperature data at the South Buoy station. Horizontal black line indicates limit of top-most RTMS measurement	142
Figure 5-76	Comparison of measured and simulated water temperature profiles at Central Buoy station in April 2013	147
Figure 5-77	Comparison of measured and simulated water salinity profiles at Central Buoy station in April 2013	147
Figure 5-78	Comparison of measured and simulated water temperature profiles at South Buoy station in April 2013	148
Figure 5-79	Comparison of measured and simulated water salinity profiles at South Buoy station in April 2013	148
Figure 5-80	Snapshot of surface velocities on 24 April 2013	149
Figure 5-81	Wind rose of BoM measurements at Garden Island between 22 and 28 April 2013	149
Figure 5-82	Comparison of simulated and measured temperature profiles at a subset of the MMMP stations on 16 April 2013	150
Figure 5-83	Comparison of simulated and measured salinity profiles at a subset of the MMMP stations on 16 April 2013	150
Figure 5-84	Comparison of simulated and measured temperature profiles at a subset of the MMMP stations on 17 April 2013	151
Figure 5-85	Comparison of simulated and measured salinity profiles at a subset of the MMMP stations on 17 April 2013	151
Figure 5-86	Comparison of simulated and measured temperature profiles at a subset of the MMMP stations on 18 April 2013	152

Contents

Figure 5-87	Comparison of simulated and measured salinity profiles at a subset of the MMMP stations on 18 April 2013	152
Figure 5-88	Comparison of simulated and measured temperature profiles at a subset of the MMMP stations on 20 April 2013	153
Figure 5-89	Comparison of simulated and measured salinity profiles at a subset of the MMMP stations on 20 April 2013	153
Figure 5-90	Comparison of simulated and measured temperature profiles at a subset of the MMMP stations on 22 April 2013	154
Figure 5-91	Comparison of simulated and measured salinity profiles at a subset of the MMMP stations on 22 April 2013	154
Figure 5-92	Comparison of simulated and measured temperature profiles at a subset of the MMMP stations on 23 April 2013	155
Figure 5-93	Comparison of simulated and measured salinity profiles at a subset of the MMMP stations on 23 April 2013	155
Figure 5-94	Comparison of simulated and measured temperature profiles at a subset of the MMMP stations on 24 April 2013	156
Figure 5-95	Comparison of simulated and measured salinity profiles at a subset of the MMMP stations on 24 April 2013	156
Figure 5-96	Comparison of simulated and measured temperature profiles at a subset of the MMMP stations on 26 April 2013	157
Figure 5-97	Comparison of simulated and measured salinity profiles at a subset of the MMMP stations on 26 April 2013	157
Figure 5-98	Comparison of simulated and measured temperature profiles at a subset of the MMMP stations on 28 April 2013	158
Figure 5-99	Comparison of simulated and measured salinity profiles at a subset of the MMMP stations on 28 April 2013	158
Figure 5-100	Comparison of simulated and measured temperature profiles at a subset of the MMMP stations on 30 April 2013	159
Figure 5-101	Comparison of simulated and measured salinity profiles at a subset of the MMMP stations on 30 April 2013	159
Figure 5-102	Comparison of simulated and measured temperature profiles measurements at either Central Buoy (25 February and 06 March) or CT7 in March 2011 (remaining profiles)	160
Figure 5-103	Comparison of simulated and measured salinity profiles at either Central Buoy (25 February and 06 March) or CT7 in March 2011 (remaining profiles)	161
Figure 5-104	Comparison of simulated and measured temperature profiles at a subset of the MMMP stations on 04 March 2011	163
Figure 5-105	Comparison of simulated and measured salinity profiles at a subset of the MMMP stations on 04 March 2011	163
Figure 5-106	Comparison of simulated and measured temperature profiles at a subset of the MMMP stations on 05 March 2011	164

Contents

Figure 5-107	Comparison of simulated and measured salinity profiles at a subset of the MMMP stations on 05 March 2011	164
Figure 5-108	Evaporation rates, wind, and relative humidity in Cockburn Sound. The negative values indicate evaporation is a flux out of the model domain.	165
Figure 5-110	Spatial distribution of <i>Fmax02</i>	167
Figure 5-110	Comparisons between simulated DO and profile measurements at North Buoy in the transition between summer and autumn 2008	170
Figure 5-111	Comparisons between simulated DO and profile measurements at Central Buoy in the transition between summer and autumn 2008	170
Figure 5-112	Comparisons between simulated DO and profile measurements at South Buoy in the transition between summer and autumn 2008	171
Figure 5-113	Simulated DO and density stratification at North Buoy in the transition between summer and autumn 2008.	171
Figure 5-114	Simulated DO and density stratification at Central Buoy in the transition between summer and autumn 2008.	172
Figure 5-115	Simulated DO and density stratification at South Buoy in the transition between summer and autumn 2008.	172
Figure 5-116	Simulated DO concentrations in Cockburn Sound illustrating near bed DO depletion in Mangles Bay. The black line in the left-hand column panes shows the plan transect of the profile presented in the right hand panes. The profiles run from northwest (left hand side) to southeast (right hand side)	173
Figure 5-117	Actual simulated sediment oxygen demand in the transition from summer to autumn 2008	174
Figure 5-118	Comparisons between simulated DO and profile measurements at North Buoy in the transition from winter to spring 2008	176
Figure 5-119	Comparisons between simulated DO and profile measurements at Central Buoy in the transition from winter to spring 2008	176
Figure 5-120	Comparisons between simulated DO and profile measurements at South Buoy in the transition from winter to spring 2008	176
Figure 5-121	Simulated DO and density stratification at North Buoy in the transition from winter to spring 2008.	177
Figure 5-122	Simulated DO and density stratification at Central Buoy in the transition from winter to spring 2008.	177
Figure 5-123	Simulated DO and density stratification at South Buoy in the transition from winter to spring 2008.	178
Figure 5-124	Actual simulated sediment oxygen demand in the transition from winter to spring 2008	179
Figure 5-125	Model predictive skill statistics for DO profiles at North Buoy (top and bottom values)	181
Figure 5-126	Model predictive skill statistics for DO profiles at Central Buoy (top and bottom values)	181

Contents

Figure 5-127	Model predictive skill statistics for DO profiles at South Buoy (top and bottom values)	181
Figure 5-128	Comparisons between simulated DO and profile measurements at Central Buoy in the transition between summer and autumn 2013	184
Figure 5-129	Comparisons between simulated DO and profile measurements at South Buoy in the transition between summer and autumn 2008	184
Figure 5-130	Comparison of simulated and measured DO profiles at a subset of the MMMP stations on 16 April 2013	185
Figure 5-131	Comparison of simulated and measured DO profiles at a subset of the MMMP stations on 17 April 2013	185
Figure 5-132	Comparison of simulated and measured DO profiles at a subset of the MMMP stations on 18 April 2013	186
Figure 5-133	Comparison of simulated and measured DO profiles at a subset of the MMMP stations on 20 April 2013	186
Figure 5-134	Comparison of simulated and measured DO profiles at a subset of the MMMP stations on 22 April 2013	187
Figure 5-135	Comparison of simulated and measured DO profiles at a subset of the MMMP stations on 23 April 2013	187
Figure 5-136	Comparison of simulated and measured DO profiles at a subset of the MMMP stations on 24 April 2013	188
Figure 5-137	Comparison of simulated and measured DO profiles at a subset of the MMMP stations on 26 April 2013	188
Figure 5-138	Comparison of simulated and measured DO profiles at a subset of the MMMP stations on 28 April 2013	189
Figure 5-139	Comparison of simulated and measured DO profiles at a subset of the MMMP stations on 30 April 2013	189
Figure 5-140	Example colour contour pane. It presents modelled salinity so would be the centre pane in the corresponding figure	191
Figure 5-141	Temperature results – 16 April 2013 (field, model, tracer)	192
Figure 5-142	Temperature results – 17 April 2013 (field, model, tracer)	193
Figure 5-143	Temperature results – 18 April 2013 (field, model, tracer)	194
Figure 5-144	Temperature results – 20 April 2013 (field, model, tracer)	195
Figure 5-145	Temperature results – 22 April 2013 (field, model, tracer)	196
Figure 5-146	Temperature results – 23 April 2013 (field, model, tracer)	197
Figure 5-147	Temperature results – 24 April 2013 (field, model, tracer)	198
Figure 5-148	Temperature results – 26 April 2013 (field, model, tracer)	199
Figure 5-149	Temperature results – 28 April 2013 (field, model, tracer)	200
Figure 5-150	Temperature results – 30 April 2013 (field, model, tracer)	201
Figure 5-151	Salinity results – 16 April 2013 (field, model, tracer)	202
Figure 5-152	Salinity results – 17 April 2013 (field, model, tracer)	203

Contents

Figure 5-153	Salinity results – 18 April 2013 (field, model, tracer)	204
Figure 5-154	Salinity results – 20 April 2013 (field, model, tracer)	205
Figure 5-155	Salinity results – 22 April 2013 (field, model, tracer)	206
Figure 5-156	Salinity results – 23 April 2013 (field, model, tracer)	207
Figure 5-157	Salinity results – 24 April 2013 (field, model, tracer)	208
Figure 5-158	Salinity results – 26 April 2013 (field, model, tracer)	209
Figure 5-159	Salinity results – 28 April 2013 (field, model, tracer)	210
Figure 5-160	Salinity results – 30 April 2013 (field, model, tracer)	211
Figure 5-161	DO results – 16 April 2013 (field, model, tracer)	212
Figure 5-162	DO results – 17 April 2013 (field, model, tracer)	213
Figure 5-163	DO results – 18 April 2013 (field, model, tracer)	214
Figure 5-164	DO results – 20 April 2013 (field, model, tracer)	215
Figure 5-165	DO results – 22 April 2013 (field, model, tracer)	216
Figure 5-166	DO results – 23 April 2013 (field, model, tracer)	217
Figure 5-167	DO results – 24 April 2013 (field, model, tracer)	218
Figure 5-168	DO results – 26 April 2013 (field, model, tracer)	219
Figure 5-169	DO results – 28 April 2013 (field, model, tracer)	220
Figure 5-170	DO results – 30 April 2013 (field, model, tracer)	221
Figure 5-172	MMMP salinity measurements – 16 th April 2013	223
Figure 5-173	Modelled salinity – 16 th April 2013	224
Figure 5-174	MMMP salinity measurements – 20 th April 2013	225
Figure 5-175	Modelled salinity – 20 th April 2013	226
Figure 5-176	MMMP salinity measurements – 28 ^h April 2013	227
Figure 5-177	Modelled salinity – 28 th April 2013	228
Figure 5-177	Comparison of simulated and measured DO profiles measurements at either Central Buoy (25 February and 06 March) or CT7 in March 2011 (remaining profiles)	229
Figure 5-178	Comparison of simulated and measured DO profiles at a subset of the MMMP stations on 04 March 2011	231
Figure 5-179	Comparison of simulated and measured DO profiles at a subset of the MMMP stations on 05 March 2011	232
Figure 5-180	Meteorological and oceanographical data in Cockburn Sound in November 2015. a) BoM Garden Island wind speed. b) BoM Garden Island wind direction. c) BoM Garden Island air temperature. d) CFSR mean sea level pressure. e) HYCOM + NCODA mean water surface level. The hatched area shows the dates associated with the fish kill event.	234
Figure 5-181	Simulated temperature profiles with and without inclusion of the PSDP intake and discharge at Central Buoy station in November 2015	236

Contents

Figure 5-182	Simulated temperature profiles with and without inclusion of the PSDP intake and discharge at South Buoy station in November 2015	236
Figure 5-183	Simulated salinity profiles with and without inclusion of the PSDP intake and discharge at Central Buoy station in November 2015	237
Figure 5-184	Simulated salinity profiles with and without inclusion of the PSDP intake and discharge at South Buoy station in November 2015	237
Figure 5-185	Simulated DO profiles with and without inclusion of the PSDP intake and discharge at Central Buoy station in November 2015	238
Figure 5-186	Simulated DO profiles with and without inclusion of the PSDP intake and discharge at South Buoy station in November 2015	238
Figure 5-187	Temperature, salinity and DO at the upper and lower-most cells of the model for November 2015 simulations with and without the PSDP discharge	240
Figure 5-188	Simulation results from 05 to 10 November 2015. Top left: near bed temperature. Filled dot points show Central and South Buoy locations. The jagged line from north to south shows the location of the curtains presented in the centre panels. The “boomerang” shaped line shows the curtains along Callista and Stirling Channels on the right-hand panels. The open circles indicate the start of the curtains. Middle left: near bed salinity. Bottom left: near bed DO. Top centre: north-south temperature curtain. Middle centre: north-south salinity curtain. Bottom centre: north-south DO curtain. Top right: along channels temperature curtain. Middle right: along channels salinity curtain. Bottom right: along channels DO curtain. Inset shows water surface elevations at South Buoy and the wind intensity and direction in Cockburn Sound.	242
Figure 5-189	Simulation results from 18 to 23 November 2015. Top left: near bed temperature. Filled dot points show Central and South Buoy locations. The jagged line from north to south shows the location of the curtains presented in the centre panels. The “boomerang” shaped line shows the curtains along Callista and Stirling Channels on the right-hand panels. The open circles indicate the start of the curtains. Middle left: near bed salinity. Bottom left: near bed DO. Top centre: north-south temperature curtain. Middle centre: north-south salinity curtain. Bottom centre: north-south DO curtain. Top right: along channels temperature curtain. Middle right: along channels salinity curtain. Bottom right: along channels DO curtain. Inset shows water surface elevations at South Buoy and the wind intensity and direction in Cockburn Sound.	254
Figure A-1	Effluent plume resulting from CFD simulations. Results depict the 1:10 iso-surface dilution.	A-2
Figure A-2	Effluent plume resulting from CFD simulations. Results depict the 1:20 iso-surface dilution.	A-3
Figure A-3	Effluent plume resulting from CFD simulations. Results depict the 1:30 iso-surface dilution.	A-4
Figure A-4	Effluent plume resulting from CFD simulations. Results depict the 1:40 iso-surface dilution.	A-5
Figure A-5	Effluent plume resulting from CFD simulations. Results depict the 1:50 iso-surface dilution	A-6

Contents

Figure C-1	Three-dimensional dilution field. Colour represents a dilution iso-surface of 1:20 for a depth-averaged ambient velocity of 0.03 m/s in the southwest direction	C-2
Figure C-2	Schematic of the Translation of the Nearfield Weighting Functions (W_j) into the Farfield Model	C-4
Figure E-1	Comparison between simulated velocities and ADCP measurements at Spoil Grounds for May to July 2006	E-2
Figure E-2	Comparison between simulated velocities and ADCP measurements at 5.1m from sea bed at Spoil Grounds for May to July 2006	E-3
Figure E-3	Comparison between simulated velocities and ADCP measurements at 3.6m from sea bed at Spoil Grounds for May to July 2006	E-3
Figure E-4	Comparison between simulated velocities and ADCP measurements at 1.6m from sea bed at Spoil Grounds for May to July 2006	E-3
Figure E-5	Comparison between simulated velocities and ADCP measurements at Spoil Grounds for 10 May to 24 May 2006	E-4
Figure E-6	Comparison between simulated velocities and ADCP measurements at 5.1m from sea bed at Spoil Grounds for 10 May to 24 May 2006	E-5
Figure E-7	Comparison between simulated velocities and ADCP measurements at 3.6m from sea bed at Spoil Grounds for 10 May to 24 May 2006	E-5
Figure E-8	Comparison between simulated velocities and ADCP measurements at 1.6m from sea bed at Spoil Grounds for 10 May to 24 May 2006	E-5
Figure E-9	Comparison between simulated velocities and ADCP measurements at Spoil Grounds for 24 May to 7 June 2006	E-6
Figure E-10	Comparison between simulated velocities and ADCP measurements at 5.1m from sea bed at Spoil Grounds for 24 May to 7 June 2006	E-7
Figure E-11	Comparison between simulated velocities and ADCP measurements at 3.6m from sea bed at Spoil Grounds for 24 May to 7 June 2006	E-7
Figure E-12	Comparison between simulated velocities and ADCP measurements at 1.6m from sea bed at Spoil Grounds for 24 May to 7 June 2006	E-7
Figure E-13	Comparison between simulated velocities and ADCP measurements at Spoil Grounds for 7 June to 21 June 2006	E-8
Figure E-14	Comparison between simulated velocities and ADCP measurements at 5.1m from sea bed at Spoil Grounds for 7 June to 21 June 2006	E-9
Figure E-15	Comparison between simulated velocities and ADCP measurements at 3.6m from sea bed at Spoil Grounds for 7 June to 21 June 2006	E-9
Figure E-16	Comparison between simulated velocities and ADCP measurements at 1.6m from sea bed at Spoil Grounds for 7 June to 21 June 2006	E-9
Figure E-17	Comparison between simulated velocities and ADCP measurements at Spoil Grounds for 21 June to 5 June 2006	E-10
Figure E-18	Comparison between simulated velocities and ADCP measurements at 5.1m from sea bed at Spoil Grounds for 21 June to 5 July 2006	E-11

Contents

Figure E-19	Comparison between simulated velocities and ADCP measurements at 3.6m from sea bed at Spoil Grounds for 21 June to 5 July 2006	E-11
Figure E-20	Comparison between simulated velocities and ADCP measurements at 1.6m from sea bed at Spoil Grounds for 21 June to 5 July 2006	E-11
Figure E-21	Comparison between simulated velocities and ADCP measurements at Spoil Grounds for 5 June to 7 June 2006	E-12
Figure E-22	Comparison between simulated velocities and ADCP measurements at 5.1m from sea bed at Spoil Grounds for 5 July to 7 July 2006	E-13
Figure E-23	Comparison between simulated velocities and ADCP measurements at 3.6m from sea bed at Spoil Grounds for 5 July to 7 July 2006	E-13
Figure E-24	Comparison between simulated velocities and ADCP measurements at 1.6m from sea bed at Spoil Grounds for 5 July to 7 July 2006	E-13
Figure E-25	Comparison between simulated velocities and ADCP measurements at Northern Basin for May to July 2006	E-14
Figure E-26	Comparison between simulated velocities and ADCP measurements at 15.5m from sea bed at Northern Basin for May to July 2006	E-15
Figure E-27	Comparison between simulated velocities and ADCP measurements at 9.5m from sea bed at Northern Basin for May to July 2006	E-15
Figure E-28	Comparison between simulated velocities and ADCP measurements at 2.5m from the sea bed at Northern Basin for May to July 2006	E-15
Figure E-29	Comparison between simulated velocities and ADCP measurements at Northern Basin for 10 May to 24 May 2006	E-16
Figure E-30	Comparison between simulated velocities and ADCP measurements at 15.5m from sea bed at Northern Basin for 10 May to 24 May 2006	E-17
Figure E-31	Comparison between simulated velocities and ADCP measurements at 9.5m from sea bed at Northern Basin for 10 May to 24 May 2006	E-17
Figure E-32	Comparison between simulated velocities and ADCP measurements at 2.5m from sea bed at Northern Basin for 10 May to 24 May 2006	E-17
Figure E-33	Comparison between simulated velocities and ADCP measurements at Northern Basin for 24 May to 7 June 2006	E-18
Figure E-34	Comparison between simulated velocities and ADCP measurements at 15.5m from sea bed at Northern Basin for 24 May to 7 June 2006	E-19
Figure E-35	Comparison between simulated velocities and ADCP measurements at 9.5m from sea bed at Northern Basin for 24 May to 7 June 2006	E-19
Figure E-36	Comparison between simulated velocities and ADCP measurements at 2.5m from sea bed at Northern Basin for 24 May to 7 June 2006	E-19
Figure E-37	Comparison between simulated velocities and ADCP measurements at Northern Basin for 7 June to 21 June 2006	E-20
Figure E-38	Comparison between simulated velocities and ADCP measurements at 15.5m from sea bed at Northern Basin for 7 June to 21 June 2006	E-21
Figure E-39	Comparison between simulated velocities and ADCP measurements at 9.5m from sea bed at Northern Basin for 7 June to 21 June 2006	E-21

Contents

Figure E-40	Comparison between simulated velocities and ADCP measurements at 2.5m from sea bed at Northern Basin for 7 June to 21 June 2006	E-21
Figure E-41	Comparison between simulated velocities and ADCP measurements at Northern Basin for 21 June to 5 July 2006	E-22
Figure E-42	Comparison between simulated velocities and ADCP measurements at 15.5m from sea bed at Northern Basin for 21 June to 5 July 2006	E-23
Figure E-43	Comparison between simulated velocities and ADCP measurements at 9.5m from sea bed at Northern Basin for 21 June to 5 July 2006	E-23
Figure E-44	Comparison between simulated velocities and ADCP measurements at 2.5m from sea bed at Northern Basin for 21 June to 5 July 2006	E-23
Figure E-45	Comparison between simulated velocities and ADCP measurements at Northern Basin for 5 July to 7 July 2006	E-24
Figure E-46	Comparison between simulated velocities and ADCP measurements at 15.5m from sea bed at Northern Basin for 5 July to 7 July 2006	E-25
Figure E-47	Comparison between simulated velocities and ADCP measurements at 9.5m from sea bed at Northern Basin for 5 July to 7 July 2006	E-25
Figure E-48	Comparison between simulated velocities and ADCP measurements at 2.5m from sea bed at Northern Basin for 5 July to 7 July 2006	E-25
Figure E-49	Comparison between simulated velocities and ADCP measurements at Spoil Grounds for February to March 2007	E-26
Figure E-50	Comparison between simulated velocities and ADCP measurements at 5.6m from sea bed at Spoil Grounds for February to March 2007	E-27
Figure E-51	Comparison between simulated velocities and ADCP measurements at 4.1m from sea bed at Spoil Grounds for February to March 2007	E-27
Figure E-52	Comparison between simulated velocities and ADCP measurements at 2.1m from sea bed at Spoil Grounds for February to March 2007	E-27
Figure E-53	Comparison between simulated velocities and ADCP measurements at Spoil Grounds for 1 February to 14 February 2007	E-28
Figure E-54	Comparison between simulated velocities and ADCP measurements at 5.6m from sea bed at Spoil Grounds for 1 February to 14 February 2007	E-29
Figure E-55	Comparison between simulated velocities and ADCP measurements at 4.1m from sea bed at Spoil Grounds for 1 February to 14 February 2007	E-29
Figure E-56	Comparison between simulated velocities and ADCP measurements at 2.1m from sea bed at Spoil Grounds for 1 February to 14 February 2007	E-29
Figure E-57	Comparison between simulated velocities and ADCP measurements at Spoil Grounds for 14 February to 28 February 2007	E-30
Figure E-58	Comparison between simulated velocities and ADCP measurements at 5.6m from sea bed at Spoil Grounds for 14 February to 28 February 2007	E-31
Figure E-59	Comparison between simulated velocities and ADCP measurements at 4.1m from sea bed at Spoil Grounds for 14 February to 28 February 2007	E-31
Figure E-60	Comparison between simulated velocities and ADCP measurements at 2.1m from sea bed at Spoil Grounds for 14 February to 28 February 2007	E-31

Contents

Figure E-61	Comparison between simulated velocities and ADCP measurements at Spoil Grounds for 28 February to 14 March 2007	E-32
Figure E-62	Comparison between simulated velocities and ADCP measurements at 5.6m from sea bed at Spoil Grounds for 28 February to 14 March 2007	E-33
Figure E-63	Comparison between simulated velocities and ADCP measurements at 4.1m from sea bed at Spoil Grounds for 28 February to 14 March 2007	E-33
Figure E-64	Comparison between simulated velocities and ADCP measurements at 2.1m from sea bed at Spoil Grounds for 28 February to 14 March 2007	E-33
Figure E-65	Comparison between simulated velocities and ADCP measurements at Spoil Grounds for 14 March to 28 March 2007	E-34
Figure E-66	Comparison between simulated velocities and ADCP measurements at 5.6m from sea bed at Spoil Grounds for 14 March to 28 March 2007	E-35
Figure E-67	Comparison between simulated velocities and ADCP measurements at 4.1m from sea bed at Spoil Grounds for 14 March to 28 February 2007	E-35
Figure E-68	Comparison between simulated velocities and ADCP measurements at 2.1m from sea bed at Spoil Grounds for 14 March to 28 March 2007	E-35
Figure E-69	Comparison between simulated velocities and ADCP measurements at Spoil Grounds for 28 March to 30 March 2007	E-36
Figure E-70	Comparison between simulated velocities and ADCP measurements at 5.6m from sea bed at Spoil Grounds for 28 March to 30 March 2007	E-37
Figure E-71	Comparison between simulated velocities and ADCP measurements at 4.1m from sea bed at Spoil Grounds for 28 March to 30 March 2007	E-37
Figure E-72	Comparison between simulated velocities and ADCP measurements at 2.1m from sea bed at Spoil Grounds for 28 March to 30 March 2007	E-37
Figure E-73	Comparison between simulated velocities and ADCP measurements at Northern Basin for February to March 2007	E-38
Figure E-74	Comparison between simulated velocities and ADCP measurements at 16.5m from sea bed at Northern Basin for February to March 2007	E-39
Figure E-75	Comparison between simulated velocities and ADCP measurements at 9.5m from sea bed at Northern Basin for February to March 2007	E-39
Figure E-76	Comparison between simulated velocities and ADCP measurements at 3.5m from sea bed at Northern Basin for February to March 2007	E-39
Figure E-77	Comparison between simulated velocities and ADCP measurements at Spoil Grounds for 1 February to 14 February 2007	E-40
Figure E-78	Comparison between simulated velocities and ADCP measurements at 16.5m from sea bed at Northern Basin for 1 February to 14 February 2007	E-41
Figure E-79	Comparison between simulated velocities and ADCP measurements at 9.5m from sea bed at Northern Basin for 1 February to 14 February 2007	E-41
Figure E-80	Comparison between simulated velocities and ADCP measurements at 3.5m from sea bed at Northern Basin for 1 February to 14 February 2007	E-41
Figure E-81	Comparison between simulated velocities and ADCP measurements at Spoil Grounds for 14 February to 28 February 2007	E-42

Contents

Figure E-82	Comparison between simulated velocities and ADCP measurements at 16.5m from sea bed at Northern Basin for 14 February to 28 February 2007	E-43
Figure E-83	Comparison between simulated velocities and ADCP measurements at 9.5m from sea bed at Northern Basin for 14 February to 28 February 2007	E-43
Figure E-84	Comparison between simulated velocities and ADCP measurements at 3.5m from sea bed at Northern Basin for 14 February to 28 February 2007	E-43
Figure E-85	Comparison between simulated velocities and ADCP measurements at Spoil Grounds for 28 February to 14 March 2007	E-44
Figure E-86	Comparison between simulated velocities and ADCP measurements at 16.5m from sea bed at Northern Basin for 28 February to 14 March 2007	E-45
Figure E-87	Comparison between simulated velocities and ADCP measurements at 9.5m from sea bed at Northern Basin for 28 February to 14 March 2007	E-45
Figure E-88	Comparison between simulated velocities and ADCP measurements at 3.5m from sea bed at Northern Basin for 28 February to 14 March 2007	E-45
Figure E-89	Comparison between simulated velocities and ADCP measurements at Spoil Grounds for 14 March to 28 March 2007	E-46
Figure E-90	Comparison between simulated velocities and ADCP measurements at 16.5m from sea bed at Northern Basin for 14 March to 28 March 2007	E-47
Figure E-91	Comparison between simulated velocities and ADCP measurements at 9.5m from sea bed at Northern Basin for 14 March to 28 March 2007	E-47
Figure E-92	Comparison between simulated velocities and ADCP measurements at 3.5m from sea bed at Northern Basin for 14 March to 28 March 2007	E-47
Figure E-93	Comparison between simulated velocities and ADCP measurements at Spoil Grounds for 28 March to 30 March 2007	E-48
Figure E-94	Comparison between simulated velocities and ADCP measurements at 16.5m from sea bed at Northern Basin for 28 March to 30 March 2007	E-49
Figure E-95	Comparison between simulated velocities and ADCP measurements at 9.5m from sea bed at Northern Basin for 28 March to 30 March 2007	E-49
Figure E-96	Comparison between simulated velocities and ADCP measurements at 3.5m from sea bed at Northern Basin for 28 March to 30 March 2007	E-49
Figure G-1	Model comparisons against RTMS data at North Buoy 01 to 15 January 2008	G-1
Figure G-2	Model comparisons against RTMS data at North Buoy 15 to 29 January 2008	G-2
Figure G-3	Model comparisons against RTMS data at North Buoy 29 January to 12 February 2008	G-2
Figure G-4	Model comparisons against RTMS data at North Buoy 12 to 26 February 2008	G-3
Figure G-5	Model comparisons against RTMS data at North Buoy 26 February to 11 March 2008	G-3
Figure G-6	Model comparisons against RTMS data at North Buoy 11 to 25 March 2008	G-4
Figure G-7	Model comparisons against RTMS data at North Buoy 25 March to 01 April 2008	G-4

Contents

Figure G-8	Model comparisons against RTMS data at Central Buoy 01 to 15 January 2008	G-5
Figure G-9	Model comparisons against RTMS data at Central Buoy 15 to 29 January 2008	G-5
Figure G-10	Model comparisons against RTMS data at Central Buoy 29 January to 12 February 2008	G-6
Figure G-11	Model comparisons against RTMS data at Central Buoy 12 to 26 February 2008	G-6
Figure G-12	Model comparisons against RTMS data at Central Buoy 26 February to 11 March 2008	G-7
Figure G-13	Model comparisons against RTMS data at Central Buoy 11 to 25 March 2008	G-7
Figure G-14	Model comparisons against RTMS data at Central Buoy 25 March to 01 April 2008	G-8
Figure G-15	Model comparisons against RTMS data at South Buoy 01 to 15 January 2008	G-9
Figure G-16	Model comparisons against RTMS data at South Buoy 15 to 29 January 2008	G-9
Figure G-17	Model comparisons against RTMS data at South Buoy 29 January to 12 February 2008	G-10
Figure G-18	Model comparisons against RTMS data at South Buoy 12 to 26 February 2008	G-10
Figure G-19	Model comparisons against RTMS data at South Buoy 26 February to 11 March 2008	G-11
Figure G-20	Model comparisons against RTMS data at South Buoy 11 to 25 March 2008	G-11
Figure G-21	Model comparisons against RTMS data at South Buoy 25 March to 01 April 2008	G-12
Figure G-22	Model comparisons against RTMS data at North Buoy 01 to 15 August 2008	G-13
Figure G-23	Model comparisons against RTMS data at North Buoy 15 to 29 August 2008	G-13
Figure G-24	Model comparisons against RTMS data at North Buoy 29 August to 12 September 2008	G-14
Figure G-25	Model comparisons against RTMS data at North Buoy 12 to 26 September 2008	G-14
Figure G-26	Model comparisons against RTMS data at North Buoy 26 September to 10 October 2008	G-15
Figure G-27	Model comparisons against RTMS data at North Buoy 10 to 24 October 2008	G-15
Figure G-28	Model comparisons against RTMS data at North Buoy 24 October to 01 November 2008	G-16
Figure G-29	Model comparisons against RTMS data at Central Buoy 01 to 15 August 2008	G-17
Figure G-30	Model comparisons against RTMS data at Central Buoy 15 to 29 August 2008	G-17
Figure G-31	Model comparisons against RTMS data at Central Buoy 29 August to 12 September 2008	G-18
Figure G-32	Model comparisons against RTMS data at Central Buoy 12 to 26 September 2008	G-18

Contents

Figure G-33	Model comparisons against RTMS data at Central Buoy 26 September to 10 October 2008	G-19
Figure G-34	Model comparisons against RTMS data at Central Buoy 10 to 24 October 2008	G-19
Figure G-35	Model comparisons against RTMS data at Central Buoy 24 October to 01 November 2008	G-20
Figure G-36	Model comparisons against RTMS data at South Buoy 01 to 15 August 2008	G-21
Figure G-37	Model comparisons against RTMS data at South Buoy 15 to 29 August 2008	G-21
Figure G-38	Model comparisons against RTMS data at South Buoy 29 August to 12 September 2008	G-22
Figure G-39	Model comparisons against RTMS data at South Buoy 12 to 26 September 2008	G-22
Figure G-40	Model comparisons against RTMS data at South Buoy 26 September to 10 October 2008	G-23
Figure G-41	Model comparisons against RTMS data at South Buoy 10 to 24 October 2008	G-23
Figure G-42	Model comparisons against RTMS data at South Buoy 24 October to 01 November 2008	G-24
Figure J-1	Comparisons between simulated and measured temperature profiles at either Central Buoy (25 February and 06 March) or CT7 in March 2011 (remaining profiles)	J-1
Figure J-2	Comparison of simulated and measured salinity profiles at either Central Buoy (25 February and 06 March) or CT7 in March 2011 (remaining profiles)	J-1
Figure J-3	Comparison of simulated and measured DO profiles at either Central Buoy (25 February and 06 March) or CT7 in March 2011 (remaining profiles)	J-2
Figure J-4	Comparison of simulated and measured temperature profiles at a subset of the MMMP stations on 01 March 2011	J-2
Figure J-5	Comparison of simulated and measured salinity profiles at a subset of the MMMP stations on 01 March 2011	J-3
Figure J-6	Comparison of simulated and measured DO profiles at a subset of the MMMP stations on 01 March 2011	J-4
Figure J-7	Comparison of simulated and measured temperature profiles at a subset of the MMMP stations on 02 March 2011	J-5
Figure J-8	Comparison of simulated and measured salinity profiles at a subset of the MMMP stations on 02 March 2011	J-6
Figure J-9	Comparison of simulated and measured DO profiles at a subset of the MMMP stations on 02 March 2011	J-7
Figure J-10	Comparison of simulated and measured temperature profiles at a subset of the MMMP stations on 03 March 2011	J-8
Figure J-11	Comparison of simulated and measured salinity profiles at a subset of the MMMP stations on 03 March 2011	J-9
Figure J-12	Comparison of simulated and measured DO profiles at a subset of the MMMP stations on 03 March 2011	J-10

Contents

Figure J-13	Comparison of simulated and measured temperature profiles at a subset of the MMMP stations on 04 March 2011	J-11
Figure J-14	Comparison of simulated and measured salinity profiles at a subset of the MMMP stations on 04 March 2011	J-12
Figure J-15	Comparison of simulated and measured DO profiles at a subset of the MMMP stations on 04 March 2011	J-13
Figure J-16	Comparison of simulated and measured temperature profiles at a subset of the MMMP stations on 05 March 2011	J-14
Figure J-17	Comparison of simulated and measured salinity profiles at a subset of the MMMP stations on 05 March 2011	J-15
Figure J-18	Comparison of simulated and measured DO profiles at a subset of the MMMP stations on 05 March 2011	J-16
Figure K-1	Salinity 16 April 2013	K-2
Figure K-2	Modelled salinity 16 April 2013	K-3
Figure K-3	Salinity 17 April 2013	K-4
Figure K-4	Modelled salinity 17 April 2013	K-5
Figure K-5	Salinity 18 April 2013	K-6
Figure K-6	Modelled salinity 18 April 2013	K-7
Figure K-7	Salinity 20 April 2013	K-8
Figure K-8	Modelled salinity 20 April 2013	K-9
Figure K-9	Salinity 22 April 2013	K-10
Figure K-10	Modelled salinity 22 April 2013	K-11
Figure K-11	Salinity 23 April 2013	K-12
Figure K-12	Modelled salinity 23 April 2013	K-13
Figure K-13	Salinity 24 April 2013	K-14
Figure K-14	Modelled salinity 24 April 2013	K-15
Figure K-15	Salinity 26 April 2013	K-16
Figure K-16	Modelled salinity 26 April 2013	K-17
Figure K-17	Salinity 28 April 2013	K-18
Figure K-18	Modelled salinity 28 April 2013	K-19
Figure K-19	Salinity 30 April 2013	K-20
Figure K-20	Modelled salinity 30 April 2013	K-21

List of Tables

Table 3-1	Model constants	45
Table 3-2	Boundary conditions considered in the CFD simulations	49

Contents

Table 3-3	Comparison of model results with Roberts and Abessi (2014) scaling	52
Table 3-4	Minimum dilutions at the end of nearfield (25.4 m from the diffuser) obtained from CFD simulations	53
Table 4-1	Available bathymetric data	56
Table 4-2	PSDP boundary specification	67
Table 4-3	Industrial discharges and intakes boundary conditions	69
Table 4-4	Summary of TUFLOW FV model configuration and parameterisations	70
Table 5-1	Calibration goals for water levels	72
Table 5-2	Error measures for water levels	80
Table 5-3	Details of ADCP arrangements	80
Table 5-4	Calibration goals for velocity	82
Table 5-5	Summary of model predictive skill statistics for currents at Spoil Grounds in Winter 2006	89
Table 5-6	Summary of model predictive skill statistics for currents at Northern Basin in Winter 2006	89
Table 5-7	Summary of model predictive skill statistics for currents at Spoil Grounds in Summer 2007	97
Table 5-8	Summary of model predictive skill statistics for currents at Northern Basin in Summer 2007	97
Table 5-9	Details of RTMS arrangements	99
Table 5-10	Calibration goals for temperature and salinity	120
Table 5-11	Summary of model predictive skill statistics for temperature at North Buoy	121
Table 5-12	Summary of model predictive skill statistics for temperature at Central Buoy	121
Table 5-13	Summary of model predictive skill statistics for temperature at South Buoy	122
Table 5-14	Calibration goals for DO	179

1 Introduction

1.1 Background

As the southwest climate of Australia continues to experience dry winter conditions, sole reliance on rainfall to meet potable water demand has necessarily become problematic, and over the last twenty years or so new water sources have therefore been sought to meet growing demand (Water Corporation 2009). For example, as part of the integrated water supply scheme of the Perth Metropolitan Area, the Perth Seawater Desalination Plant (PSDP) at Kwinana was constructed and commenced operation in November 2006. It currently contributes 45 GL per year (or approximately 18%) to Perth's total water supply (<https://www.watercorporation.com.au/water-supply/our-water-sources/desalination/perth-seawater-desalination-plant>) and discharges its saline return waters to nearby Cockburn Sound. As part of its ongoing planning, Water Corporation is currently assessing production of desalinated water over and above that currently sourced from the PSDP. One of the options being considered is an additional water extraction of 25 to 50 GL per year through desalination, also proposed for the locality of Kwinana. As such, Water Corporation commissioned BMT to develop a hydrodynamic and water quality numerical model of Cockburn Sound and its surrounds to provide a platform by which subsequent assessments of the fate and transport of return waters from the existing and proposed plant might be undertaken in future. This report details the development and calibration of these models.

1.2 Scope of this report

This report presents the setup and validation of the numerical modelling tool developed for subsequent assessment of desalination plant return water discharges to Cockburn Sound. The project scope included the following:

- A review of historical observations and modelling of the hydrodynamic conditions of Cockburn Sound and the surrounding oceanic waters;
- Setup and execution of a detailed nearfield dilution assessment using Computational Fluid Dynamics (CFD) modelling; and
- Establishment and validation of a farfield model linked to the nearfield CFD model for subsequent use in supporting assessments of current and future brine discharges in the region.

Compilation and review of available data for this assessment is contained in the Perth Desalination Plant Discharge Modelling: Data Collation Report (BMT WBM 2017a).

It is not within the scope of this report to assess suitable locations and/or impacts of the proposed desalination plant return water discharge.

2 Site characterisation

2.1 Setting and morphology

The PSDP is located within the Kwinana Industrial Area (KIA) on the eastern shore of Cockburn Sound, approximately 38 km south of the Perth CBD (Figure 2-1), Western Australia. Cockburn Sound is a semi-enclosed embayment bounded by the Australian mainland to the east and south, and Garden Island to the west. The main opening to the Sound is to the north between Woodman Point (east) and the northeast tip of Garden Island. A causeway linking Rockingham to the southern end of Garden Island completes the western boundary of the Sound. This causeway was completed in 1974 and contains two openings that are approximately 300 m and 600 m wide.

Cockburn Sound covers approximately 110 km² and extends approximately 15 km from north to south and 9 km from east to west at its widest point. The width reduces to the south, being approximately 5 km between the Causeway and East Rockingham. The Sound can be split into two main bathymetric regions, those being a deep central basin (covering approximately 60% of the Sound's area) with depths between 17.0 and 22.0 m, and a shallower shore area with depths of up to 12.0 m. This shallower region covers approximately 40% of the Sound's area and is particularly prominent along its eastern boundary (Figure 2-2).

Waters immediately north of the Sound (i.e. between Carnac Island and Owen Anchorage) sit on a sill that is relatively shallow with depths ranging between 2.0 and 5.0 m. Success and Parmelia Channels (with depths of approximately 15.0 m) are routinely dredged to allow shipping traffic in and out of Cockburn Sound. A range of dredged shipping channels inside the Sound provides access to local industrial berths, including Woodman, Jervoise, Medina, Calista and Stirling Channels. In particular, Calista and Stirling Channels are relevant to the movement of the PSDP brine effluent in Cockburn Sound (CWR 2007).

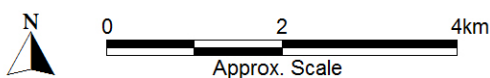


Title:
Perth Seawater Desalination Plant and Outfall Locality

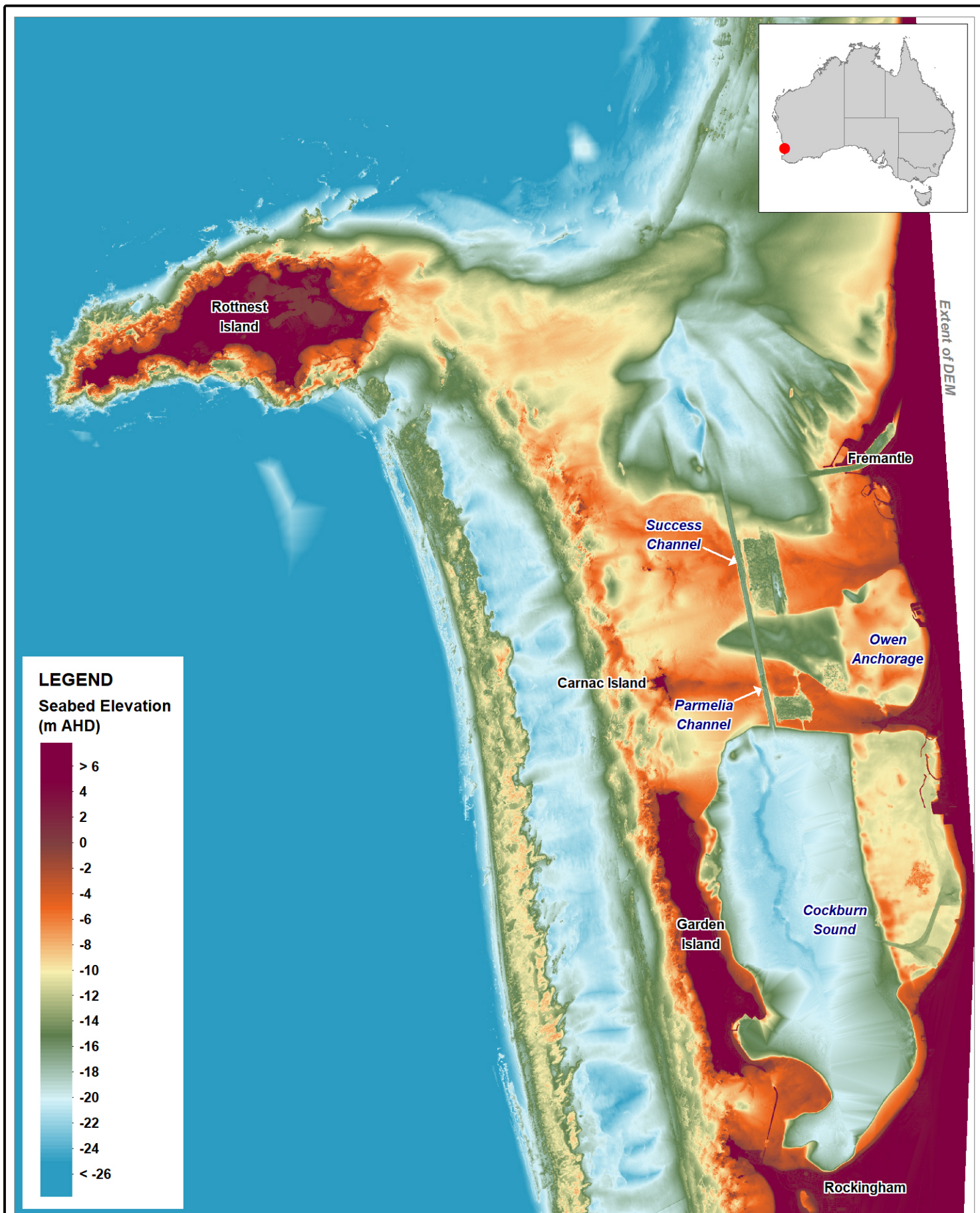
Figure:
2-1

Rev:
A

BMT WBM endeavours to ensure that the information provided in this map is correct at the time of publication. BMT WBM does not warrant, guarantee or make representations regarding the currency and accuracy of information contained in this map.



Filepath: I:\B22253.I.meb.CockburnSound\DRG\CAR_003_170926_Perth Seawater Desalination Plant and Outfall Locality.wor



Title:
Digital Elevation Model of Cockburn Sound and Surrounds

Figure:

2-2

Rev:

A

BMT WBM endeavours to ensure that the information provided in this map is correct at the time of publication. BMT WBM does not warrant, guarantee or make representations regarding the currency and accuracy of information contained in this map.



0 4 8km
Approx. Scale



Filepath: I:\B22253.I.meb.CockburnSound\DRG\CAR_011_171003_Digital Elevation Model of Cockburn Sound.wor

Site characterisation

2.2 Meteorology and hydrodynamics

2.2.1 Climate drivers

It has been well established that climate drivers influence strongly the hydrodynamic and ecological behaviour of environmental waterways (Evans et al. 2017). How these drivers might interact to generate potentially adverse hydrodynamic and water quality conditions is particularly relevant to Cockburn Sound (BMT 2017) and this scope of works. Given this, the salient aspects of the climatic patterns of Southwest Western Australia are described following. A detailed description of these patterns in the Perth area and Cockburn Sound is provided in D'Adamo (2002), such that only the key aspects thereof are discussed here.

2.2.1.1 General

Perth's climate is described as Mediterranean with dry hot summer months and wet cool winters. This climate interplay results primarily from the seasonally varying latitudinal position of the subtropical anticyclonic high pressure belt (also referred to as the "subtropical ridge"), as described below. The barometric variations within the subtropical ridge have a period of approximately one week, which is reflected in the 7 to 10 days recurrence of synoptic weather patterns in the southwest of Australia (D'Adamo, 2002).

2.2.1.2 Summer to Early Autumn Climate

Between late September and May, and more notably in summer and early autumn (December to March), the subtropical ridge moves further south (approximately between 40 and 50 degrees latitude) whilst the monsoon trough (low pressure band nearing the equator) is drawn towards the north of Australia. The combination of the weather systems in association with the heating of air over the land produces warm easterly winds at the latitudes of Cockburn Sound (Kepert and Smith 1992). These winds are typically of the order of 5 m/s and are generally active in the morning periods (D'Adamo 1992). With diurnal heating in summer, the temperature difference between land and sea drives a pressure gradient producing a (usually afternoon) sea breeze. Over most of Western Australia's coastline the sea breeze moves in an alongshore direction (Masselink and Pattiaratchi 2001) and for Cockburn Sound, it means that under the influence of the Earth's rotation, the wind direction is from the south to southwest. Although the sea breeze in Perth is a year-round feature, it is more prevalent and energetic in the summer months and is responsible for producing strong northward currents along the coastline from afternoon to the early evening (Masselink and Pattiaratchi 2001).

Kepert and Smith (1992) showed that a combination of the warm easterly winds with the cool sea breezes form the main mechanism for generation of the West Coast trough, which is a low-pressure band with an axis aligned from north to south of Western Australia, generally characterised by weak warm north-easterly winds. The position of the West Coast trough determines the intensity at which the sea breeze operates in the coastal regions of southern Western Australia (Kepert and Smith 1992). When the trough forms inland, the sea breezes are more active in the coastal area, form earlier in the day and bring some respite for local air temperatures. Under these conditions, the wind velocities of the sea breeze are typically of 8 to 10 m/s, but can be as high as 15 m/s (D'Adamo 1992). Conversely, when the West Coast trough forms offshore, it acts as a blockage of oceanic

Site characterisation

airflow, and the corresponding sea breezes are weaker (and sometimes may not even form). Sea breezes also start developing later in the day and do not advance far inland. Under this meteorological setting, calm conditions at the coast prevail and (noting that air temperatures to the east of the low are elevated) air temperatures across Perth can exceed 40 °C. If the low becomes stationary in the ocean for a two- to three-day period, a heat wave may result (Kepert and Smith 1992). As frontal systems move from west to east with the synoptic weather patterns, the West Coast trough moves inland and loses its structure, culminating in the re-establishment of the land and sea breeze pattern discussed earlier.

In addition to the climate drivers described above, the occurrence of Tropical Cyclones (TC) in the Timor Sea and eastern Indian Ocean influence the hydrodynamics of Western Australian coastal waters. From November through to April the cyclone season may see as many as ten cyclones develop in the northwest of Australia with different intensities and paths (Elliot and Pattiaratchi 2010). Whilst the direct effects of wind and surges generated from cyclones are typically local, there is evidence that TCs give rise to coastal shelf waves (CSWs) that travel over the coastal shelf with larger nearshore than offshore amplitudes. In Western Australia, CSWs travel southwards along the entire length of its coastline (Elliot and Pattiaratchi 2010). The impacts of these waves on Perth coastal waters are described below.

An example of the climate processes and features identified above (e.g. positioning of the sub-tropical ridge and monsoon trough, passage of low and high-pressure systems, land and sea breezes, West Coast trough, tropical cyclones) is illustrated by the series of synoptic charts presented in Figure 2-3. The corresponding measured wind characteristics and air temperature at Cockburn Sound (BoM station ID 009256 at Garden Island - Figure 2-4) is presented in Figure 2-5. Each panel in Figure 2-3 is a snapshot of the BoM synoptic charts at 8:00 AM (local time) of each day between 28 February and 11 March 2008. Each of the climate drivers identified in Figure 2-3 is also annotated in Figure 2-5, so that the corresponding effect in Cockburn Sound can be distinguished. In all panels of Figure 2-3 the monsoon trough can be seen to be generally sitting at 1000 to 1010 hPa isobar. Early in the period, on 28 and 29 February, the West Coast trough was present offshore and directly over the coast (Figure 2-3, panels A and B). As a result, a westward breeze of approximately 6 m/s associated with a sharp rise in temperature on 28 February was seen in the Sound, following a shift to lower temperatures and weak winds from northeast and north (Figure 2-5, annotated 'West Coast trough offshore and over the coastline').

Between 01 and 04 March, a frontal system moved eastward and south of the Australian mainland, and in doing so dissipated the West Coast trough (Figure 2-3, panels C to F). The passage of this front produced winds from the south and southwest directions with intensities between 9 and 12 m/s (Figure 2-5, yellow areas annotated 'Passage of a frontal system'). At the same time, TC Ophelia formed in the Kimberley Coast and migrated west, veering along the northwest coast before becoming a tropical low near Carnarvon on 07 March (Figure 2-3, panels D to I). Before the veering of TC Ophelia on 03 and 04 March, a land and sea breeze pattern of winds oscillating between 3 to 6 m/s from the east at night and morning, and winds of 9 to 10 m/s from the southwest in the afternoon was established (Figure 2-5, blue areas annotated 'Land and sea breezes') over Cockburn Sound. Subsequently, and into the following day, the wind intensity reduced to 3 to 6 m/s between 05 and 07 March, without a clear directional pattern (Figure 2-5, yellow areas annotated 'Tropical cyclone influence'). A cold front associated with a cut-off low passed through the coast on 08 March (Figure

Site characterisation

2-3, panel J) producing eastward winds and reduced air temperatures (Figure 2-5, blue area annotated 'Passage of a frontal system'). Following the passage of the frontal system and without the presence of a West Coast trough, the land and sea breeze pattern re-established on 09 and 10 March producing the relatively weak (3 to 6 m/s) easterly night and morning winds and strong south-westerlies between 9 and 12 m/s (Figure 2-5, yellow areas annotated 'Land and sea breezes').

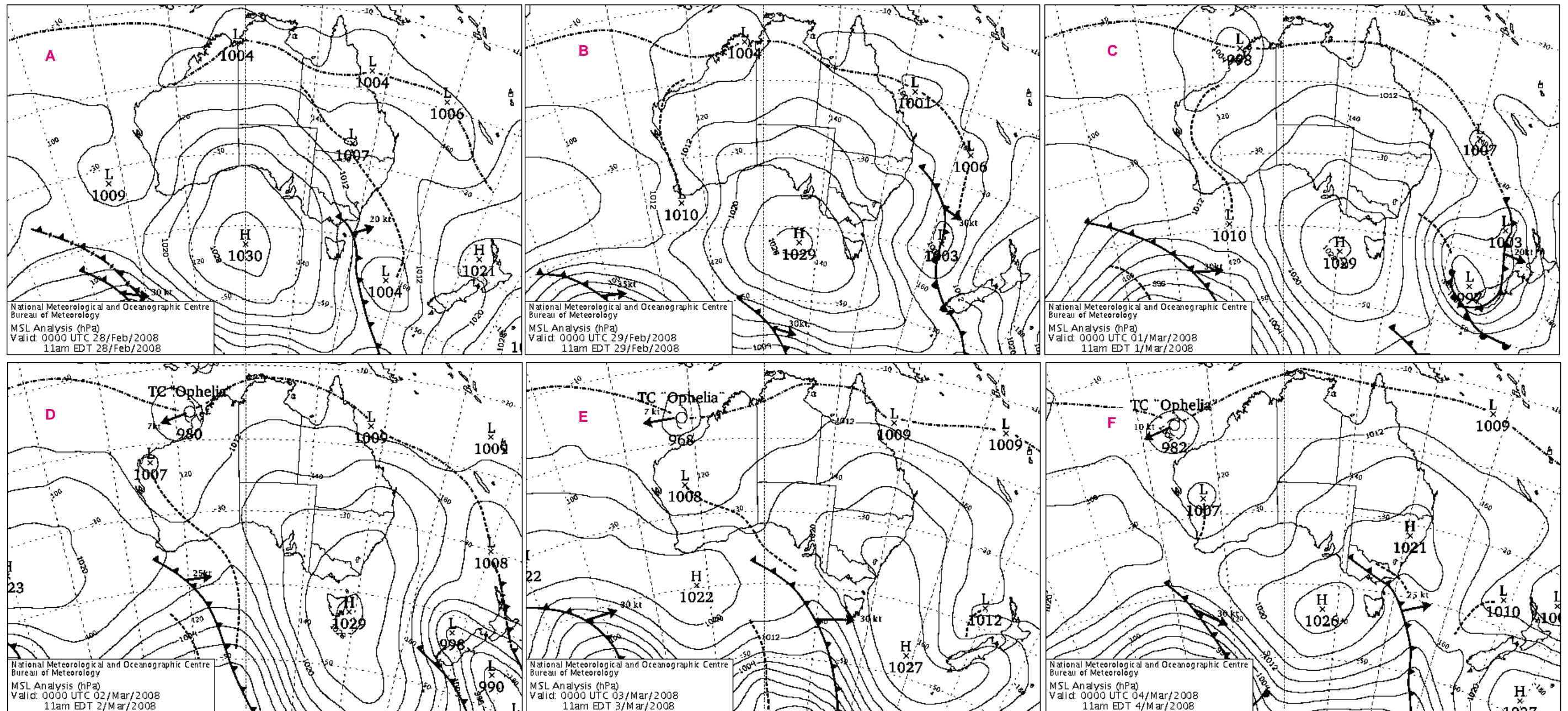


Figure 2-3 Sequence of synoptic weather charts between 28 February and 11 March 2008 (Panels A to L). Same period as in Figure 2-5. Graphs accessed from the BoM web site.

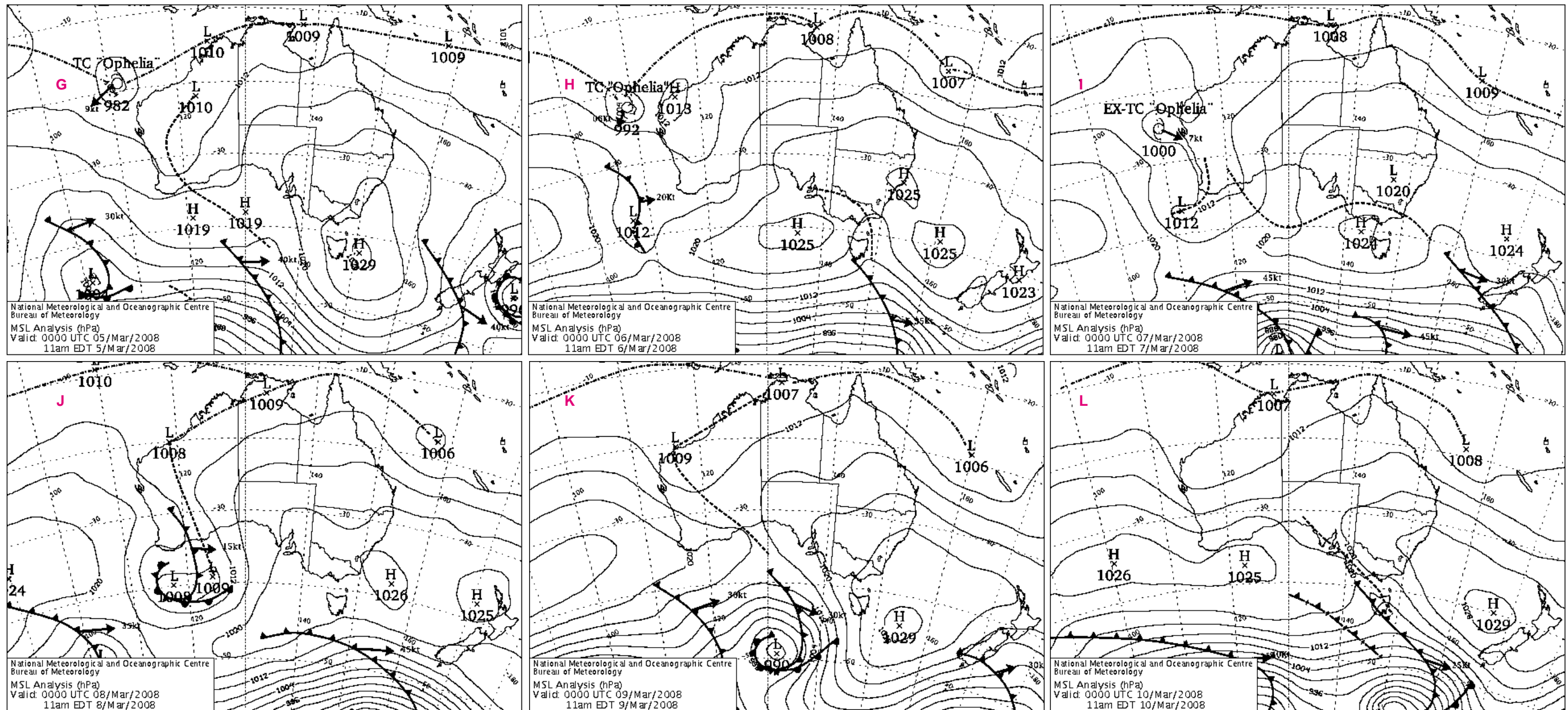


Figure 2-3 (Continued).



Title:

Meteorological and sampling stations in Cockburn Sound

Figure:

2-4

Rev:

A

BMT WBM endeavours to ensure that the information provided in this map is correct at the time of publication. BMT WBM does not warrant, guarantee or make representations regarding the currency and accuracy of information contained in this map.



0 2 4km
Approx. Scale



Filepath: I:\B22253.I.meb.CockburnSound\DRG\CAR_006_170929_Sampling Stations in Cockburn Sound.wor

Site characterisation

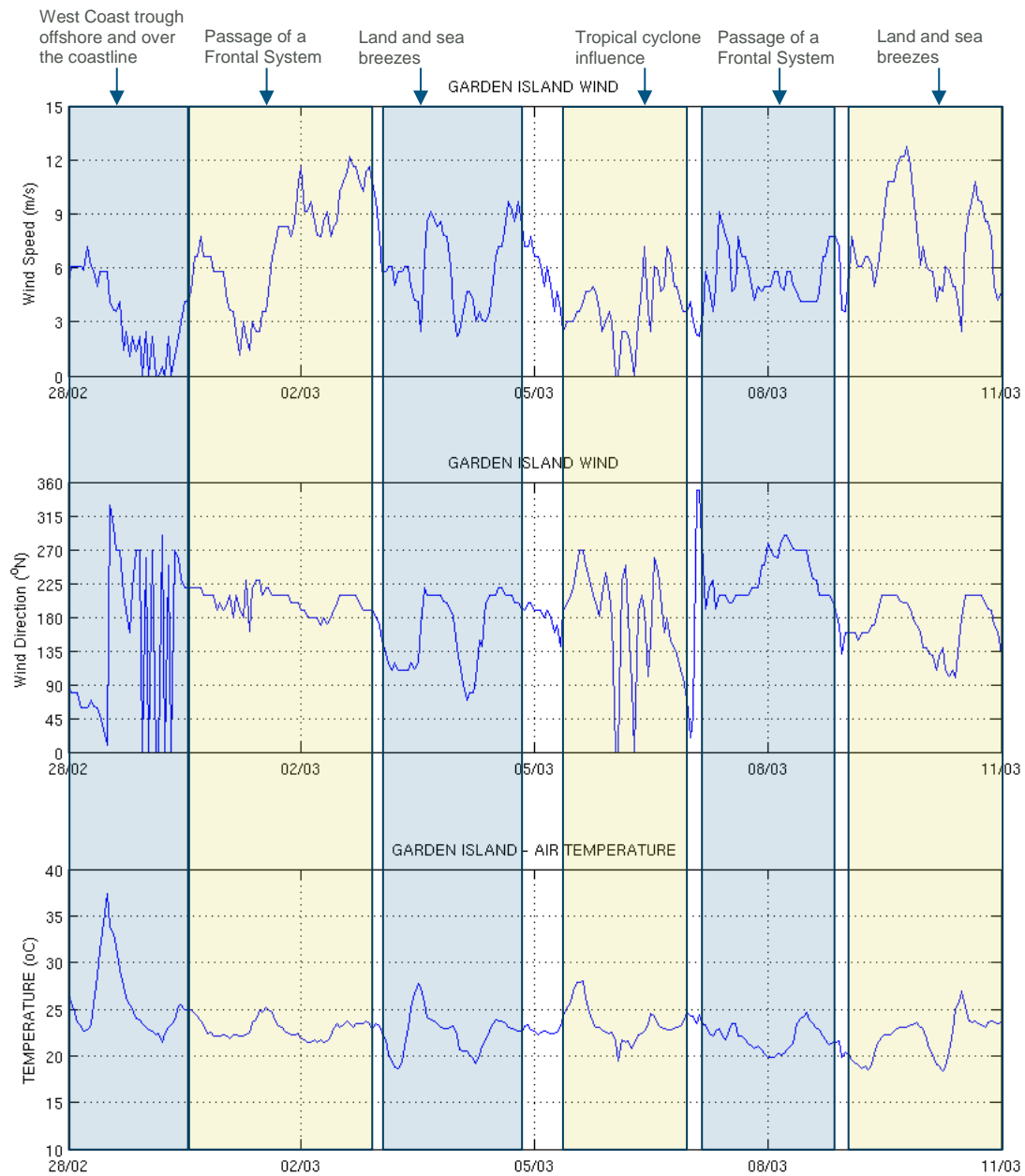


Figure 2-5 Wind and Air temperature at Garden Island: 28 February and 11 March 2008

Site characterisation

2.2.1.3 Autumn to Early Spring Climate

From autumn (March to May) through to winter (June to August), the intensity of the sea breeze over Perth coastal waters progressively diminishes (Pattiaratchi and Masselink 2001; D'Adamo 2002). As winter approaches, higher wind intensity is associated more with the passage of cold fronts (low-pressure systems) approaching from the southwest, commonly producing rainfall as they cross the coastline. As the fronts pass over the southwest of Australia, winds curl from the northwest to southwest with velocities from 10 to 15 m/s (D'Adamo 2002).

The cold fronts are a recurring pattern at every 7 to 10 days in winter and often come in two or three bouts, with one shortly after another (D'Adamo 2002). In between storms, high-pressure systems cross the southwest of Western Australia from west to east. During the passage of these systems, prevailing winds reflect the translation of the anticyclonic subtropical ridge further north, with the high-pressure zones generally sitting at higher latitudes than Cockburn Sound. These winds are generally much weaker than during storms (<7.5 m/s) but depend on the latitudinal position of the high-pressure system. D'Adamo (2002) cites an analysis that calm periods between storms in winter lasted between 1 and 24 days.

An example of the climate processes and features identified above (e.g. positioning of the subtropical ridge, passage of low- and high-pressure systems, as well as associated rainfall) is presented in Figure 2-6. The corresponding wind, air temperature and rainfall at Cockburn Sound (BoM station id 009256 at Garden Island) is shown in Figure 2-7. Similarly to Figure 2-3, each panel in Figure 2-6 presents a snapshot of the BoM synoptic charts at 8:00 AM of each day between 21 July and 05 August 2008. Again, each of the climate drivers identified in Figure 2-6 is also annotated in Figure 2-7, so the corresponding effect in Cockburn Sound can be identified. The start of the period (21 and 22 July) saw the passage of a high-pressure cell with its core drifting southeast into the continent (Figure 2-6, panels A and B). The wind activity over the time was relatively calm, and consisted of low velocities (< 5 m/s) from northeast through to southeast (Figure 2-7, blue area annotated 'High-pressure system moving across Western Australia'). The wind intensity then progressively increased to up to 10 m/s (Figure 2-7, yellow area annotated 'Low-pressure system associated with intense rainfall') with the approach of the first of the four low-pressure systems that crossed Cockburn Sound over the period (Figure 2-6, panels C and D). The passage of this low-pressure system presented much of the wind pattern characteristics described above, notably the transition from northerly winds blowing as the wind intensified, followed by sustained winds from the west and southwest. Rainfall ensued following the passage of the system through the coastline (Figure 2-7). Across the four low-pressure systems identified over the period, a total of 82 mm of rainfall were recorded at the BoM station at Garden Island (Figure 2-7), with July 2008 being the fourth wettest month on record.

Over the period, another three high-pressure systems crossed the Western Australian coast, including the time between 25 and 26 July (Figure 2-6, panels E and F), between 31 July and 01 August (Figure 2-6, panels K and L), and from 03 to 05 August (Figure 2-6, panels N and O), all showing moderate winds generally below 6 m/s and varied wind directions (Figure 2-7, areas annotated 'High-pressure system between storms'). Air temperatures as the high-pressure systems crossed the coast reduced by 2 to 8 °C in comparison to the preceding air temperatures (Figure 2-7, areas annotated 'High-pressure system between storms'). Interspersed between these high-pressure systems, the other three low-pressure systems crossed Cockburn Sound, the first two in

Site characterisation

quick succession between 27 July and 01 August (Figure 2-6, panels G to J) with peak wind speeds of 12 and 15 m/s; both systems delivered winds from the north in the early stages and transitioned through westerly and north-westerly directions (Figure 2-7, yellow area annotated 'Two low-pressure systems in succession'). The third low-pressure system that crossed Cockburn Sound on 02 August (Figure 2-6, panel M) showed a pattern as described earlier, with winds curling from the northwest to southwest with a peak velocity of 12 m/s (Figure 2-7, yellow area annotated 'Low-pressure system').

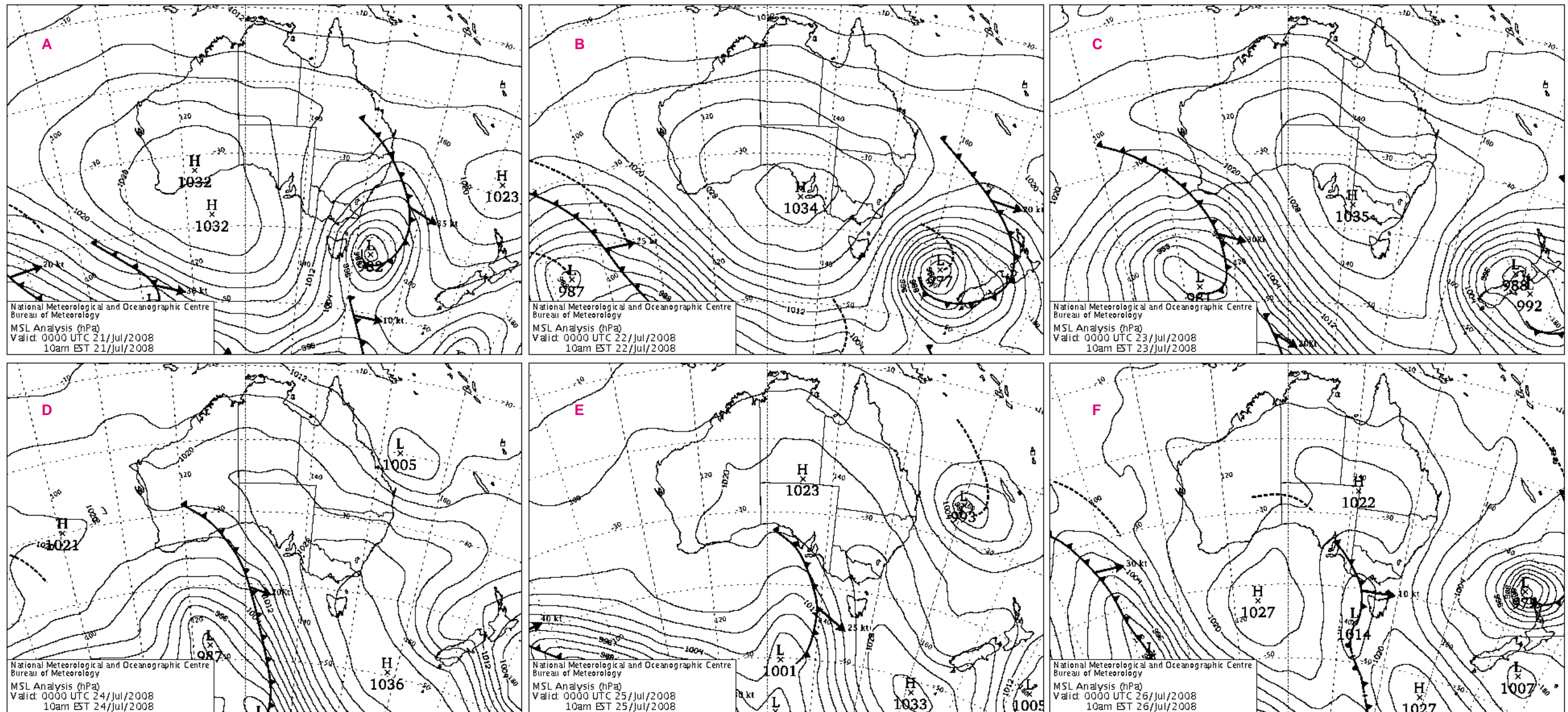


Figure 2-6 Sequence of synoptic weather charts between 21 July and 05 August 2008 (Panels A to O). Same period in Figure 2-7. Graphs accessed from the BoM web site.

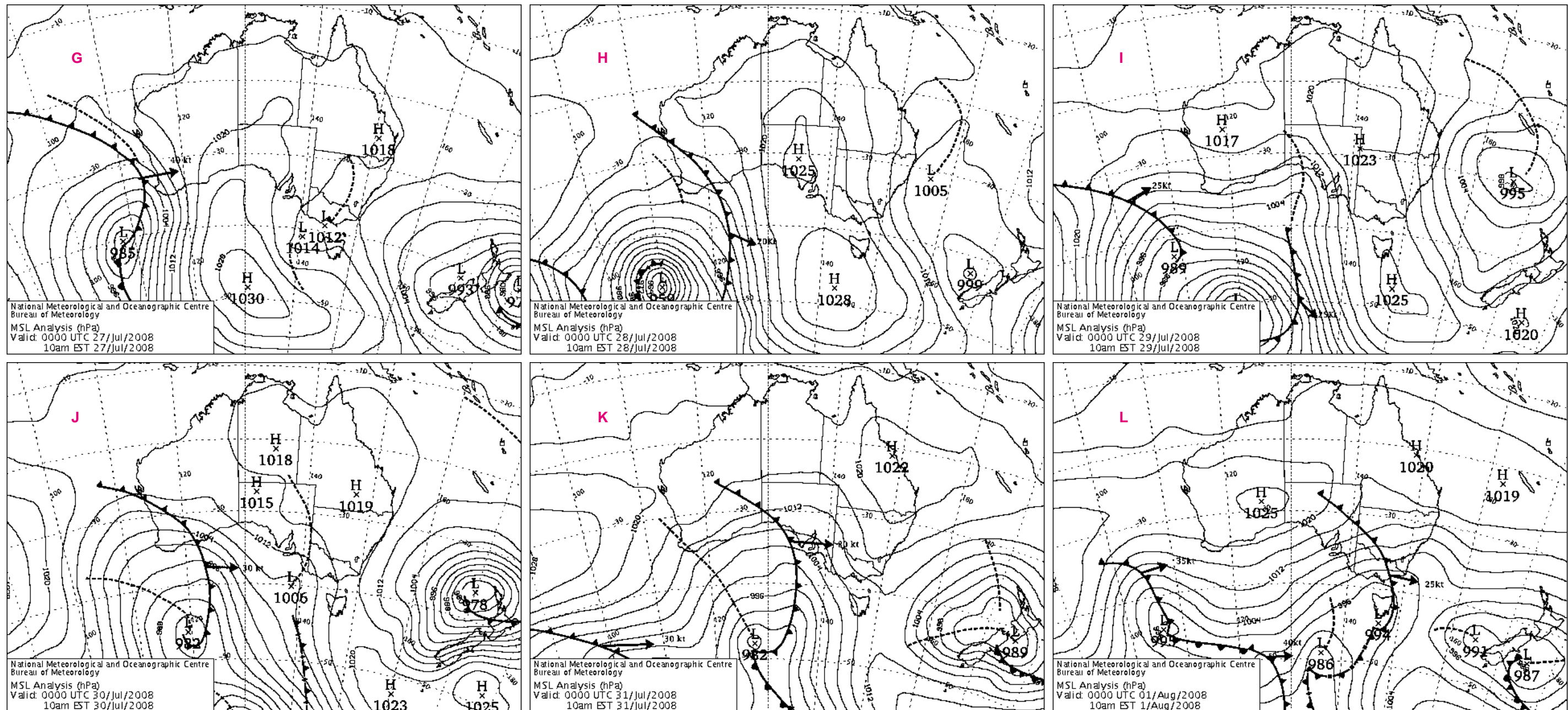


Figure 2-6 (continued)

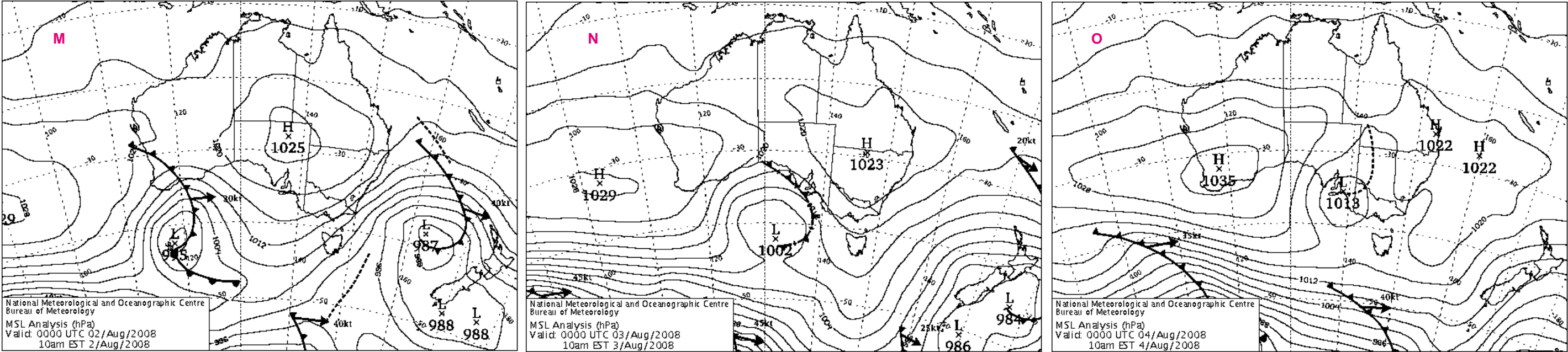


Figure 2-6 (continued)

Site characterisation

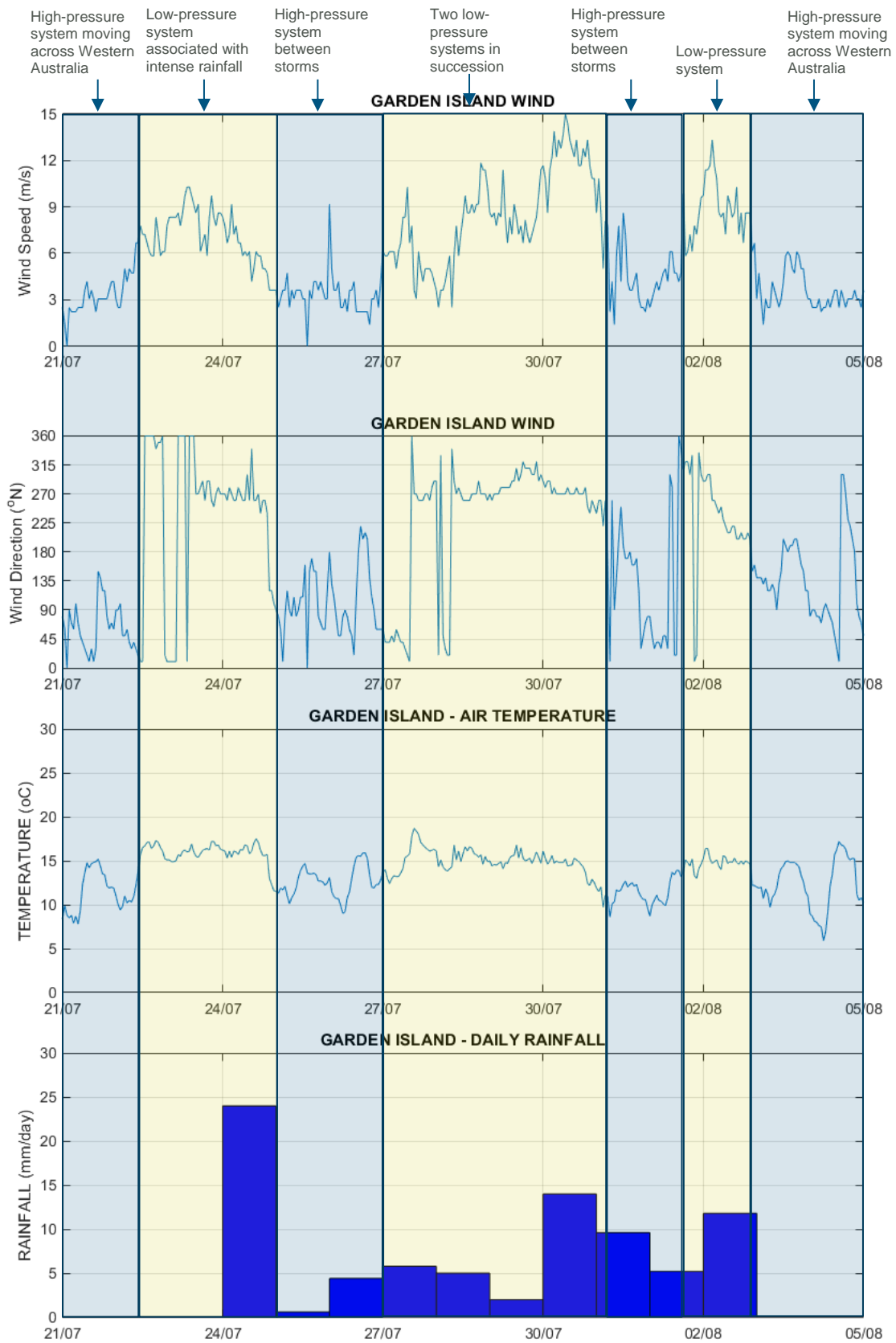


Figure 2-7 Wind, Air temperature and Rainfall at Garden Island: 21 July to 05 August 2008

Site characterisation

2.2.2 Hydrodynamics

The hydrodynamics of Cockburn Sound are largely influenced by the climate drivers described above (together of course with other drivers such as tidal processes). Additionally, the semi-enclosed nature of the Sound's basin limits water exchange with adjacent coastal waters, particularly noting the presence of the causeway south of Garden Island and the sills and reef lines north of the Sound. The primary hydrodynamic processes of Cockburn Sound are described below.

2.2.2.1 Wind-driven currents

Given the relatively low-amplitude regional astronomical tides, wind is the main forcing mechanisms in Cockburn Sound. The role of the wind is twofold. Firstly, wind directly exerts stress on the water surface and therefore drives surface water motion within the Sound. Secondly, wind impacts heat exchange at the atmosphere-ocean surface which in turn influences evaporation and therefore temperature and salinity fields within the Sound waters. Wind also imparts energy that can be used for water column mixing both in terms of wind stirring and wind shear.

Based on measurements in autumn of 1977 and two-dimensional (vertically-averaged) numerical model results, Steedman and Craig (1983) postulated that Cockburn Sound functioned akin to a closed system and that wind was the only mechanism capable of inducing currents above 0.10 m/s throughout the Sound. Their numerical model showed that with increasing wind speeds, two large eddies would form with flows approaching the east and west margins of the Sound in the same direction of the applied wind stress, whilst the deep basin would produce flow in the opposite direction. As such, a strong wind from the north (i.e. a typical approaching winter storm – see Figure 11 of Steedman and Craig, 1983) would create currents towards the south near the Sound margins and a northward flow out of the Sound through the central deep basin. Conversely, a strong wind from the south (i.e. from a strong sea breeze) would create currents towards the north near the Sound margins and a southward flow out of the Sound through the central deep basin (see Figure 9 of Steedman and Craig, 1983). Further, due to a break in the topography (i.e. typically south of James Point into the Southern Flats and Mangles Bay), the southern part of the Sound was more isolated with its own circulation cells rotating in the opposite direction of the eddy in the north basin.

The role of the wind in water motion can be further illustrated by the Acoustic Doppler Current Profile (ADCP) data from Fremantle Port Authority (FPA) and the BoM wind data at Garden Island (Figure 2-8 and Figure 2-9). ADCP data are presented as collected from two locations (Figure 2-4), *Northern Basin* in relatively deep water (~20.0 m depth) and *Spoil Grounds* in the transition between the shallow and deep basins (~7.0 m depth). The period comprises a 6-day calm interval (21 to 27 June) in between two storms with peak wind speeds in excess of 12 m/s (Figure 2-8). The storms approached with winds from the north shifting towards south-westerly and south directions (Figure 2-8).

In the shallow station (Spoil Grounds), as the first storm approached on 19 June, surface currents started moving south subsequently taking over the entire water column as the wind intensity increased towards 10 m/s (Figure 2-8). Over this acceleration period the current intensity was recorded to surpass 0.20 m/s (Figure 2-8). As the wind started changing direction to the west and southwest, water currents also changed their direction to be approximately the same as the wind stresses (i.e. towards east and northeast) with speeds of up to 0.10 m/s (Figure 2-8).

Site characterisation

Throughout the subsequent calm period, currents were generally below 0.05 m/s, with brief episodes of the surface layer currents reaching up to 0.12 m/s, again approximately in the same direction of the wind stress (e.g. moving northwest with a weak sea breeze on 23 June and moving southeast to south with winds from north and west on 25 and 26 June, see Figure 2-8).

The same pattern of currents then developed as the next storm approached on the 27 June, changing with the direction of the wind stress, so moving initially south and shifting to a northward direction at up to 0.20 m/s as the wind intensity reached its peak (Figure 2-8). Flow was sustained above 0.10 m/s northward on 28 June as a constant wind from the south receded to approximately 5.0 m/s (Figure 2-8).

Compared to the shallow station, flow was generally weaker and more complex in structure in the deeper station (Northern Basin - Figure 2-8). For example, a three-layer structure was observed in response to the moderate winds from the north in the calm period on 25 June and just before the second storm early on 27 June (Figure 2-8). On these occasions, the surface layer moved south to southeast at up to 0.15 m/s, whilst a return flow of up to 0.08 m/s moving west and northwest established in the lower part of the water column (Figure 2-8).

Also in contrast to the shallow station, flow in the deeper location was subject to vertical shear during the storms (Figure 2-8). For instance, over the storms on 27 and 28 June, flow in the surface layer likely surpassed 0.20 m/s (note the surface velocities were not recorded for all of the period) as the currents shifted from southeast to southwest (Figure 2-8). A strong flow (indeed stronger than at the surface) towards southeast and east at depth (up to 0.15 m/s) formed on 28 June (Figure 2-8). This indicates the flow patterns in the deeper water are more complex than the picture given by the two-dimensional model results of Steedman and Craig (1983)¹.

Contrasting to the winter period, ADCP data between 24 February and 03 March 2007 shows the response of currents to three distinct wind patterns in summer (Figure 2-9): firstly, a calm period of winds generally from the east and below 5 m/s (24 to 28 February) ensued, which is characteristic of a West Coast trough (not shown) sitting just west of the coastline; secondly, a low-pressure system (28 to 03 March – not shown) with strong winds (up to 14 m/s) passed from the north and northwest; and thirdly, the establishment of the land and sea-breeze pattern (03 to 08 March) is evident, with weak winds from the east (5 to 6 m/s) in the mornings interposed with strong (~12 m/s) to moderate (~7 m/s) winds from the south in the afternoons and evenings (Figure 2-9).

At the shallower site (Spoil Grounds), there was a clear correspondence between wind intensity and the currents across the water column (Figure 2-9). Strong and moderate winds (i.e. above 7.0 m/s) drove flow across the water column with velocities in excess of 0.07 m/s (Figure 2-9). For weaker wind intensities, the flow was generally confined to the surface layer with little or no returning current below. In particular, the sea-breeze in the end of the period could produce near surface velocities (note the data did not extend to the top of the water column) approaching 0.20 m/s flowing in a northward fashion (Figure 2-9).

At the deeper site (Northern Basin), the three-layer current structure was again evident (Figure 2-9). Over the period dominated by the land and sea-breezes, a continuous pattern with alternating light

¹ This is not a criticism of Steedman and Craig (1983) as the simplification of their results was in line with the computational limitations at the time their work was conducted.

Site characterisation

currents in the morning (westward to southward) and strong northward surface currents (sometimes in excess of 0.15 m/s) in the afternoon recurred (Figure 2-9). As the northward flows established, a current approximately in the opposite direction up to 0.08 m/s formed at mid depth and near the seabed. This pattern appeared to be reinforced each additional day the land-sea breeze system was operating, given the strongest currents were not necessarily associated with the strongest breezes (Figure 2-9).

Another feature at the shallower site (Spoil Grounds) was the influence of the Sound bathymetry in the resulting currents. For example, the currents flowed in the same direction of the wind stress for winds from south, north and east (Figure 2-9). For winds from the west or northwest direction however (such as the strong westerly and north-westerly winds sustained by the passage of the low-pressure system) currents flowed predominantly to the south and southeast (Figure 2-9). Flows were somewhat similar in the deeper site, which over this strong-wind period did not present the three-layer structure but rather moved in a similar direction and magnitude over the entire water column (Figure 2-9).

For the calm period, the currents in the deeper site (Northern Basin) were generally weak (< 0.05 m/s), however increased to ~ 0.10 m/s at the surface at both sites as the wind changed to a northerly direction (i.e. from the north, Figure 2-9). This was unlikely to be exclusively driven by the wind stresses, but rather by a combination of the adjustment of salinity gradients and the influence of low-frequency oscillations (see subsequent sections for expansion).

Site characterisation

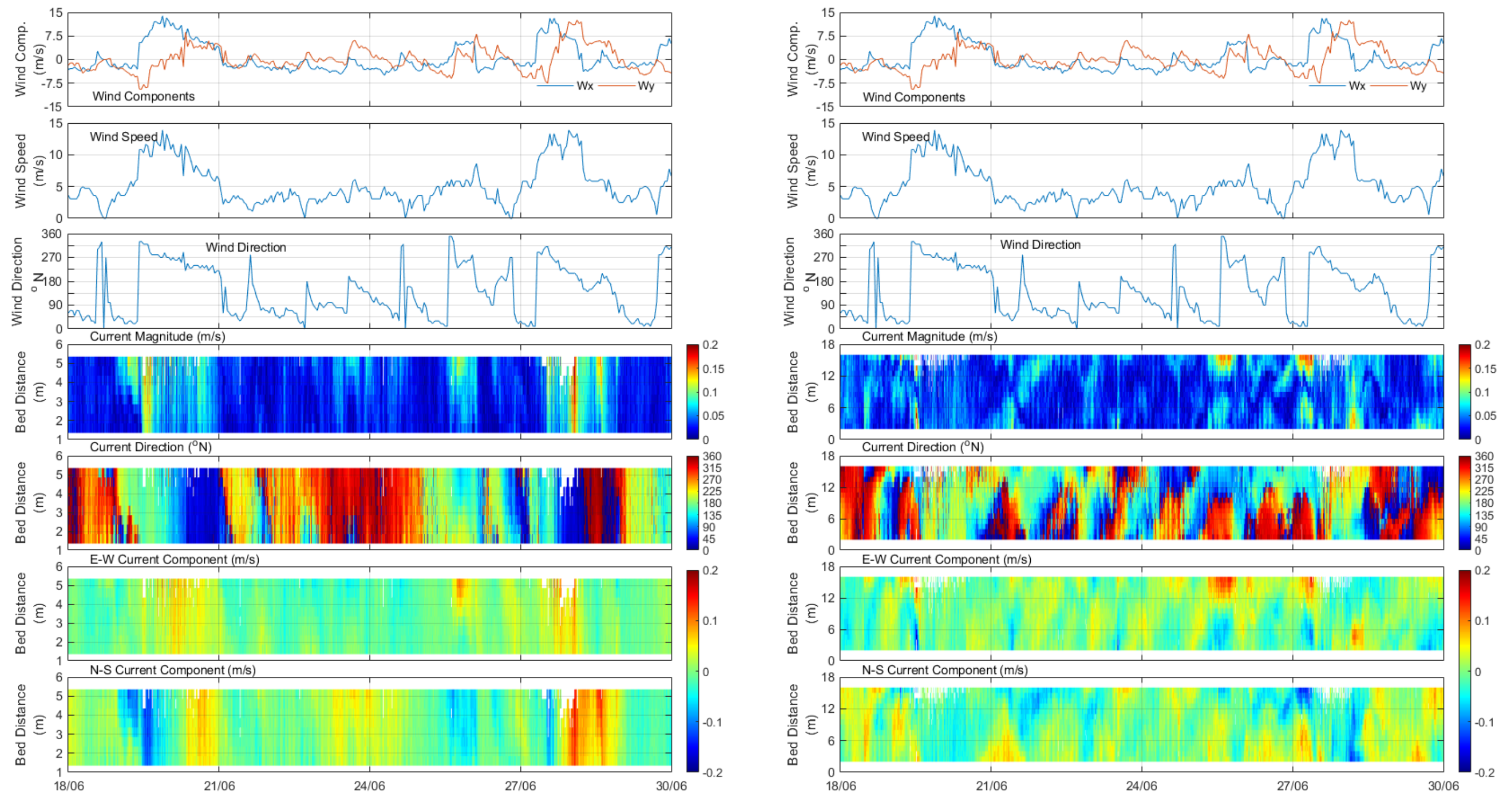


Figure 2-8 Wind field (BoM station at Gardens Island) and currents (FPA data) in Cockburn Sound from 18 and 30 June 2006. Left panels: Spoil Grounds station. Right Panel: Northern Basin station. Wind data is the same on both left and right panels.

Site characterisation

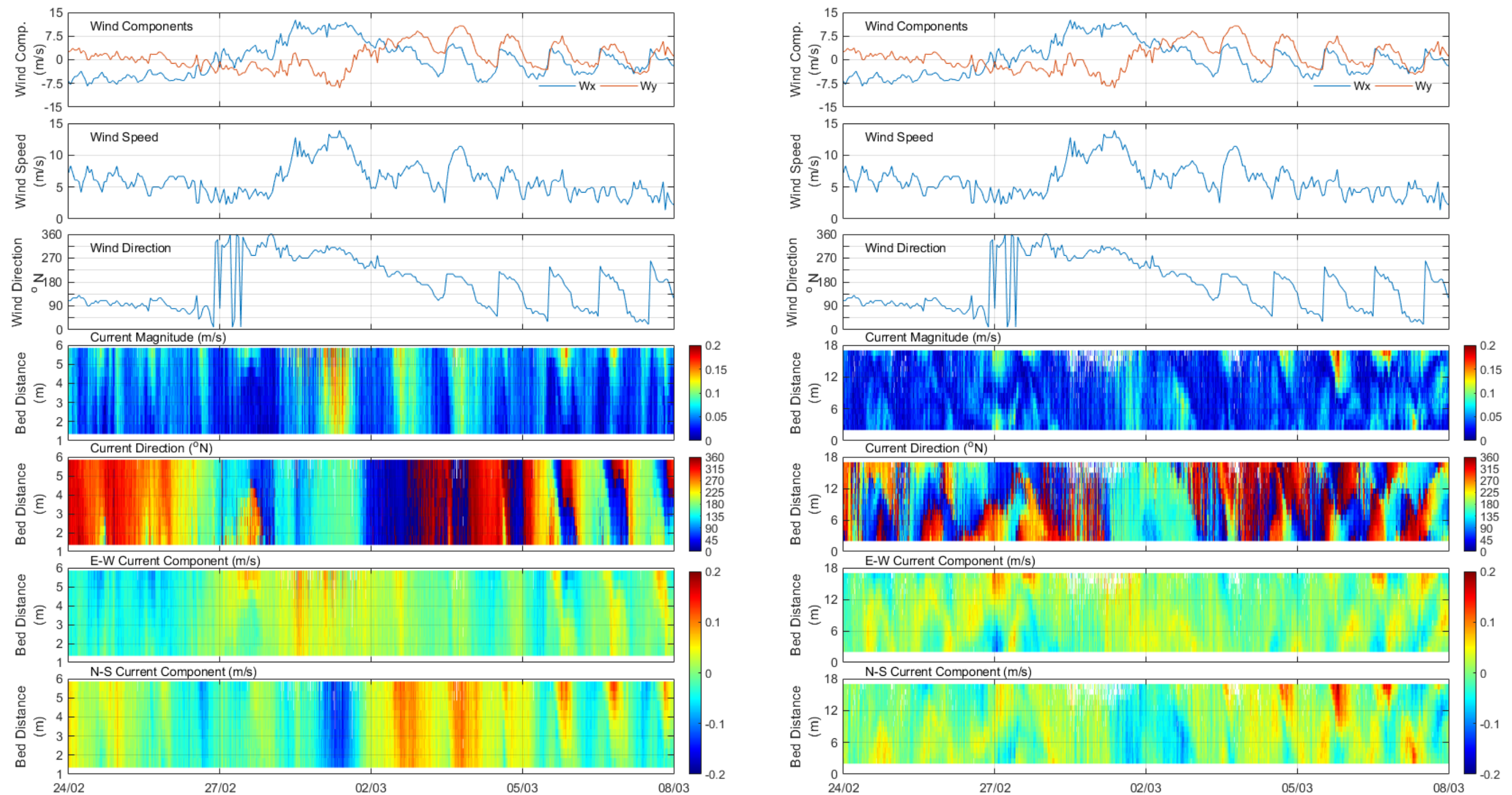


Figure 2-9 Wind field (BoM station at Gardens Island) and currents (FPA data) in Cockburn Sound from 24 March to 03 March 2007. Left panels: Spoil Grounds station. Right Panel: Northern Basin station. Wind data is the same on both left and right panels.

2.2.2.2 Density gradients

Both salinity and temperature change seasonally, but at different rates in the Sound compared to the adjacent ocean. As such, density gradients develop both horizontally and vertically between the two water bodies. The temperature-salinity diagrams presented in D'Adamo (2002) illustrate how these seasonal changes occur and how they relate to physical processes in Cockburn Sound.

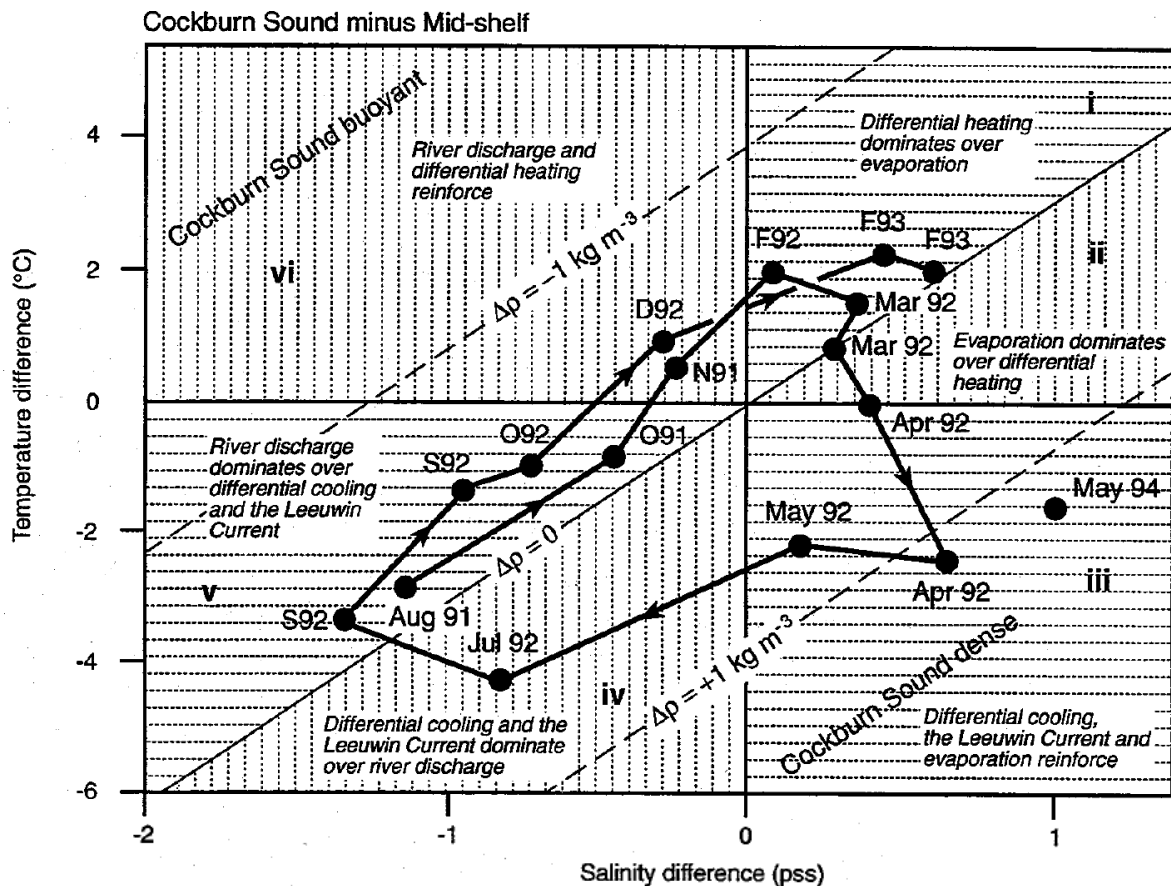


Figure 2-10 The annual cycle in the salinity and temperature differences (ΔS and ΔT , respectively) between Central Cockburn Sound and the mid shelf at 10 m depth (from D'Adamo, 2002)

Low moisture air and the sea-breeze in summer drive flow northwards and play a pivotal role in the onset of evaporation along the Perth coastline and Cockburn Sound (which can be up to approximately 10 mm/day). Evaporation then drives increased salinity in Cockburn Sound (in a similar fashion to the dynamics of inverse estuaries), as exchange with the outer ocean is limited. This is shown in Figure 2-10 as an increase in both temperature and salinity difference between November and February (see also Figure 2-12 how salinities in the Sound increased from January to March 2008). As summer transitions to autumn from February to May, the Sound cools at a faster rate and becomes appreciably denser than the adjacent waters (Figure 2-10); the magnitude of the density difference is influenced by the strength of the Leeuwin current, which is warmer and less saline (thus less dense), as it strengthens offshore of the shelf.

Site characterisation

Contrastingly, as winter approaches and rainfall increases, flows from the Swan-Canning River system become stronger, and therefore deliver freshwater to coastal waters (DEP 1996). Nearly 80% of the annual mean rainfall (870 mm) in Perth falls between May and September, with approximately 85% of the run-off originating from the Avon River (O'Callaghan et al. 2007). Peak flows in the period vary with rainfall intensity, however the total flow of the Swan River at Walyunga for a 10% annual exceedance probability is approximately 435 m³/s with a critical duration of 144 hours (HARC 2016).

Freshwater flows upon leaving the estuary are influenced by the earth's rotation, as well as winds from the north and northwest directions, typically taking 1.5 days to reach Cockburn Sound (DEP 1996). The river plume reaching the Sound contributes to reducing the salinity and density of Cockburn Sound up to a point where both temperature and salinity differences are at a minimum around July-August each year (Figure 2-10). Over the end of winter and through spring, temperature and salinity differences reduce due to the faster rate of heating in the Sound and the mixing action induced by storms (DEP 1996). Between October and December, temperature and salinity differences are at a minimum and the cycle described above repeats.

The seasonal changes in salinity, in addition to wind patterns, are an important driver of circulation in Cockburn Sound. In summer, wind during the day and penetrative convection at night are generally vigorous enough to maintain the water column mixed without significant vertical stratification (DEP 1996). However, during weaker wind periods (i.e. such as those induced by an offshore West Coast trough), these changes in salinity create horizontal density gradients that can drive both the local flow and vertical stratification. In late summer and into autumn, warmer, less saline and less dense offshore waters enter Cockburn Sound flowing over the top part of the water column, whilst the more saline Sound waters are confined by the sills at the northern opening. The less saline waters are then transported further south into the Sound until south and south-westerly winds act to dismantle the stratification and drive flows out of the Sound. The transport in and out of the Sound over this period can be further influenced by low-frequency oscillations as described in Section 2.2.2.3.

In winter and early spring, following the period of increased freshwater flows from the Swan and Canning systems, the Sound waters are generally less saline (and therefore less dense) than adjacent offshore waters. Storm activity is crucial for enhanced vertical mixing and exchange between the Sound and adjacent waters. Following the passage of storms, winds are generally too weak to counterbalance the motion exerted by the horizontal density gradients (DEP 1996). Waters offshore of the Sound then flow as plunging underflows under the influence of the Earth's rotation towards the eastern margins of the deep basin (DEP 1996).

2.2.2.3 Continental shelf waves

Continental shelf waves (CSWs) are low frequency oscillations induced by non-local forcing (i.e. wind) that propagate at the edge of the continental slope, with increased amplitude towards the coastline. These waves, when propagating at the water surface, are also termed coastal-trapped waves. Although D'Adamo (2002) indicated there was no evidence to suggest these play a role in the hydrodynamics of Cockburn Sound, more recent studies indicate that they may represent an important process within Perth's coastal waters.

Site characterisation

Elliot and Pattiaratchi (2010) showed that CSWs form along the west coast of Australia following the occurrence of tropical cyclones in the Indian Ocean off the northwest of Australia. These CSWs travel from north to south along the coastal shelf of Western Australia, have longer periods than tides (3 to 10 days), and undergo little dissipation as they travel south. Thus, CSWs can propagate long distances along the coast (> 4000 km) with speeds between 2 to 7 m/s and amplitudes of up to 0.8 m (Elliot and Pattiaratchi 2010). Noting that the tides in Perth are diurnal and have a relatively small amplitude (approximately 0.5 m on average), the energy within CSWs often exceeds that of the tides.

Whilst CSWs have not been directly linked to the hydrodynamics in Cockburn Sound, they were shown to considerably modify the tidal dynamics within the Swan River estuary, determining the position of the estuarine salt wedge (O'Callaghan et al. 2007). The net result of CSWs was to curb the river outflow as the wave crest propagated along the coast and into the estuary. Given the low-frequency of CSWs compared to the diurnal tidal frequency, the salt wedge was driven several kilometres up the river, affecting the water quality and salinity within the lower reaches of the river (O'Callaghan et al. 2007). In a similar fashion, CSWs are thought to affect the exchange of water between Cockburn Sound and its surrounding waters (C. Pattiaratchi, pers. comm.), noting that the highest salinity gradients occur at the same time CSWs are active along the Western Australian coast.

The current speed increases on 27 February 2007 under very weak wind conditions (Figure 2-9) were possibly a result of CSWs. The origin of these CSWs is not conclusive, but the period of their arrival in Cockburn Sound coincided with Tropical Cyclone Humba that formed in the Indian Ocean at approximately 80°E longitude, travelling southward from 12°S to 30°S latitude between 22 and 28 February 2007 (MMS 2008).

The signature of these CSWs is better illustrated by the tidal records at Mangles Bay (Figure 2-11). In this case, BMT undertook harmonic analyses following Pawlowicz et al. (2002), and harmonics were then subtracted from the raw tidal signal to remove the astronomical tidal components. The CSWs over the period can be seen from 25 February towards the end of the month and were characterised by amplitudes of up to 40 cm and periods (based on the time of the crests) of between 6 to 8 days. The low wind speed period shown in Figure 2-9 coincided with the arrival of the rising limb of the first wave of the observed CSWs. The currents travelling south into the Sound showed a speed increase in the surface layer at both shallow and deep stations, and a returning flow northward at depth near the bed in the deep station (Figure 2-9). As discussed above, depending on the difference of salinity between the Sound and adjacent waters, the arrival of CSWs could deliver less saline water to the Sound, thus inducing vertical stratification. The potential effects of such events on dissolved oxygen in the Sound are further discussed below.

Site characterisation

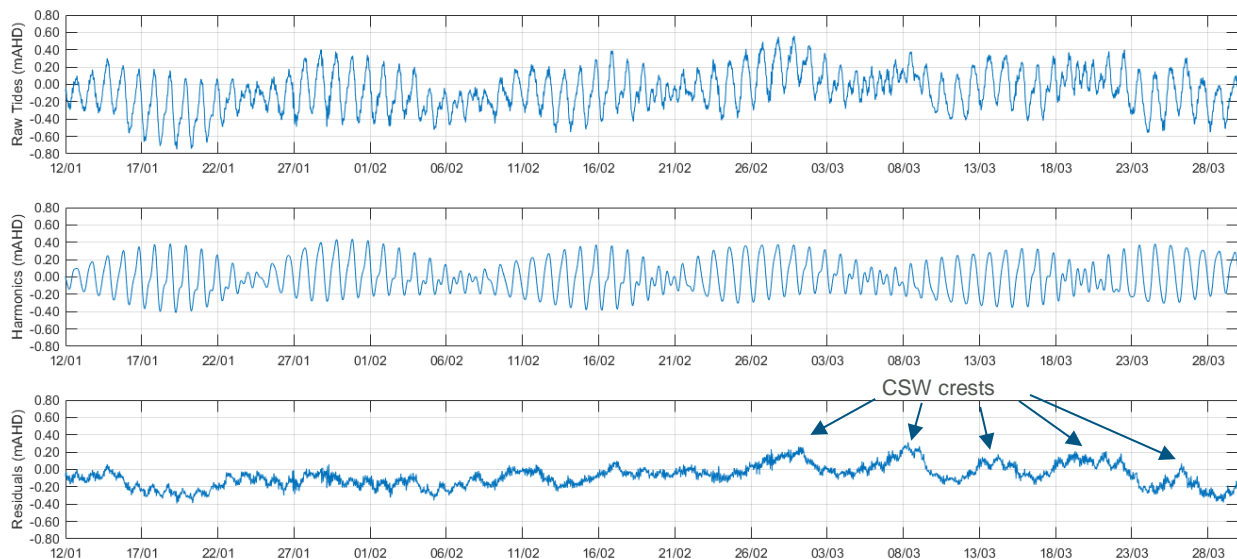


Figure 2-11 Tidal records at Mangles Bay from 12 January to 30 April 2007. Upper panel: Raw tidal record. Middle panel: harmonic components. Lower panel: residual water levels.

2.2.2.4 Secondary influences

2.2.2.4.1 Tides and waves

In comparison to the processes described above, the influence of waves and tides on Cockburn Sound hydrodynamics are of lesser importance (Steedman and Craig 1983, DEP 1996, D'Adamo 2002). Tides in Perth are mostly diurnal with relatively small amplitude (approximately 0.5 m amplitude on average - Figure 2-11), driving currents of the order of 0.01 to 0.05 m/s (D'Adamo 2002; Rose 2001). These currents are generally very small when compared to the effects of the sea breezes, storms and CSWs described above, and as such so not play a primary role in the hydrodynamics of Cockburn Sound.

Garden Island, Rottnest Island and the sills north of the Sound provide an efficient barrier to the propagation of wind waves and swell into Cockburn Sound. These high-frequency waves (i.e. in comparison to tides and CSWs) therefore play a limited role in the local hydrodynamics (D'Adamo 2002).

2.2.2.4.2 Oceanic currents

The Leeuwin-Capes currents' systems comprise another important feature of the hydrodynamics of Perth Coastal waters. The Leeuwin Current progresses southward along the West Australian coastal shelf and slope as relatively warm and low salinity flow, driven by a north to south steric height gradient, which is typically of the order of 0.55 m between approximately 10 °S and 35 °S latitudes. This current is approximately 50 to 100 km wide and about 200 m deep off the southwest coast in winter (D'Adamo 2002). The current is strongest from March to October and weakened in spring and summer months due to the south-southwest sea breezes. Over this period, the current meanders in and out of the coastal shelf. As the Leeuwin Current weakens in summer, the Capes Current

Site characterisation

strengthens flowing northwards around Cape Leeuwin (Pearce and Pattiaratchi 1998). This current has similar salinity to the southwestern waters, but is generally cooler, with waters often originating from upwelling along the south and southwestern shelves of Western Australia (Gersbach et al. 1999). This current is thought to travel all the way north to the Abrolhos Islands, which are approximately 400 km northwest of Perth. Due to the protected nature of Cockburn Sound, the Leeuwin and Capes currents exert relatively little influence on the Sound's dynamics. Steedman and Craig (1983) reasoned that whilst the temperature of near coastal waters of Perth were largely influenced by advective processes in the ocean, the temperature of water in Cockburn Sound directly responded to the atmospheric forcing, thus indicating limited influence of the large-scale currents in the Sound itself. The Leeuwin and Capes currents may contribute to dynamic changes in Cockburn Sound via altering salinity and temperature in the adjacent waters, however they are not thought to provide a direct forcing mechanism to the overall Sound circulation.

2.2.2.4.3 Surface seiches

Molloy (2001) investigated surface seiche activity in Cockburn Sound and showed they propagate along the Perth coastline at a period of approximately 2.8 to 3.0 hours. These seiches are produced by the readjustment of the water surface elevation as the wind changes direction, and are more prominent from wind changes from the west to the east coinciding with a low tide. Under the right conditions, the seiches in Cockburn Sound may reach amplitudes of up to 20 cm, noting however, their amplitudes are generally well below 10 cm (Molloy, 2001). Rose (2001) showed that although the seiche signal on water levels is significantly smaller than can tides, they have a small influence on localised currents thorough the causeway linking the mainland to Garden Island (i.e. by setting up water level differences between the Sound and the adjacent ocean water) and can therefore exert some control in the exchange of the southern waters of Cockburn Sound with the ocean. For example, effects of seiches on the flow through the causeway can be as high as 20 cm/s, whilst those of the tides are below 5 cm/s (Rose 2001). The seiche influences are, however, short-lived, lasting for no more than a day. Rose (2001) concluded their effect was secondary when compared to storms and baroclinic fluctuations, which last at similar intensities for longer periods.

2.3 Dissolved oxygen

There is a history of episodic low dissolved oxygen (DO) levels near the seabed in the deep waters of Cockburn Sound. Natural, seasonal changes in weather and marine climate trigger these low DO episodes in Cockburn Sound.

Broadly, DO concentrations in the water column are modulated through the mechanisms of surface re-aeration (turbulent diffusion across the air-water interface), production (from photosynthesis), uptake (respiration by living organisms), fluxes across the sediment-water interface and exchange with oxygen sources (e.g. adjacent waters, rivers, etc.). While DO in bottom waters is both consumed and produced by benthic biota, the dominant process is consumption, mainly by bacteria present in the sediments. This net depletion of DO at the sediment water interface is referred herein as the process of sediment oxygen demand (SOD). If water column mixing is limited and oxygen is not transported through external sources to replenish the oxygen consumed by SOD, benthic concentrations of DO can drop under the influence of this demand to levels that can be harmful to

Site characterisation

marine life (ANZECC/ARMCANZ 2000). The two most common mechanisms to transport oxygen are:

- vertical and downwards transport from the surface due to mixing driven by the wind and/or penetrative convection (i.e. movement of cooler and denser water from the surface to the bottom)
- horizontal advection (sideways currents).

One mechanism that has been identified as inhibiting this oxygen transport is vertical density stratification. Stratification is a natural phenomenon and may arise via many factors, for example: daily heating and cooling of surface waters, inflows of less dense water (rivers, groundwater, less saline and warmer oceanic waters), inflows of denser water (more saline and colder waters), and periods of prolonged light winds and high temperatures (that therefore promote surface water warming and reduced wind mixing conditions). Strong winds blowing for long enough will generally mix most naturally occurring stratifications and increase the rate of surface re-aeration. In doing so such conditions therefore promote increased oxygenation across the water column.

Due to Cockburn Sound being a semi-enclosed embayment (with much of the embayment a distance from the ocean) it has generally been assumed that oxygen levels near the seabed of the deep basin (around 20m depth) are dominated by vertical stratification and wind mixing rather than sideways advection and much of the data collected for Cockburn Sound is consistent with this wind mixing hypothesis.

Notwithstanding this, wind mixing (and therefore the vertical transport of oxygen) is ineffective when winds are light and/or the water is stratified (layers of less dense water overlies layers of denser water).

An example of how DO depletion accompanies the vertical density structure within Cockburn Sound can be seen in measurements of Water Corporation. The locations of these stations are shown in Figure 2-4 and DO, density, temperature and salinity data over summer and the early autumn of 2008 are presented in Figure 2-12. Summer through to early autumn measurements are shown as this is the period that typically presents the lowest DO concentrations, partly because DO saturation reduces with water temperature, but also because density stratification inhibits mixing of re-aerated surface waters down the water column.

Figure 2-12 also reveals that on some occasions, DO concentrations are lower at the South Buoy and vice versa at the North and Central Buoys. For example, DO concentrations in the bottom half of the water column were lower at the South Buoy on 02 January, 05 February, and 04 March. On all these occasions the level at which DO started decreasing coincided with the development of a thermocline (position of highest vertical temperature gradient), indicating local temperature stratification hindered oxygenation of bottom waters.

Contrastingly, DO concentrations were lower at both North and Central Buoys on 29 February, 01 March, 06 March, and 08 March, with lowest concentrations at the North Buoy. On these occasions, the low DO concentrations within the bottom part of the water column coincided with an observed reduction of salinity on the top part of the water column. Also, the vertical level at which DO started decreasing coincided with the position of the halocline (position of highest vertical salinity gradient), although there was also a degree of temperature stratification. Wind at Garden Island indicated that at or before these times wind was generally subdued (Figure 2-5). Noting the Swan River flow was

Site characterisation

minimal over that period, these characteristics indicated that the vertical stratification of the water column was driven by advection of offshore waters into Cockburn Sound through the northern opening. The advection resulted from a combination of the gravitational adjustment (similar to the observations and modelling of D'Adamo 2002) and the CSWs associated with the formation of TC Ophelia (Figure 2-13). The same level of density stratification was not observed at the South Buoy, indicating the southern areas of the Sound were much less influenced from the exchange of less saline waters into the Sound, and as a result, DO was therefore not as depressed at depth.

Finally, on other occasions, such as on 22 January, 19 February, and 18 March, vertical density stratification was weak and DO concentrations were homogeneous, and generally high throughout the water column. Mixing was sustained by relatively strong southerly and easterly winds (not shown).

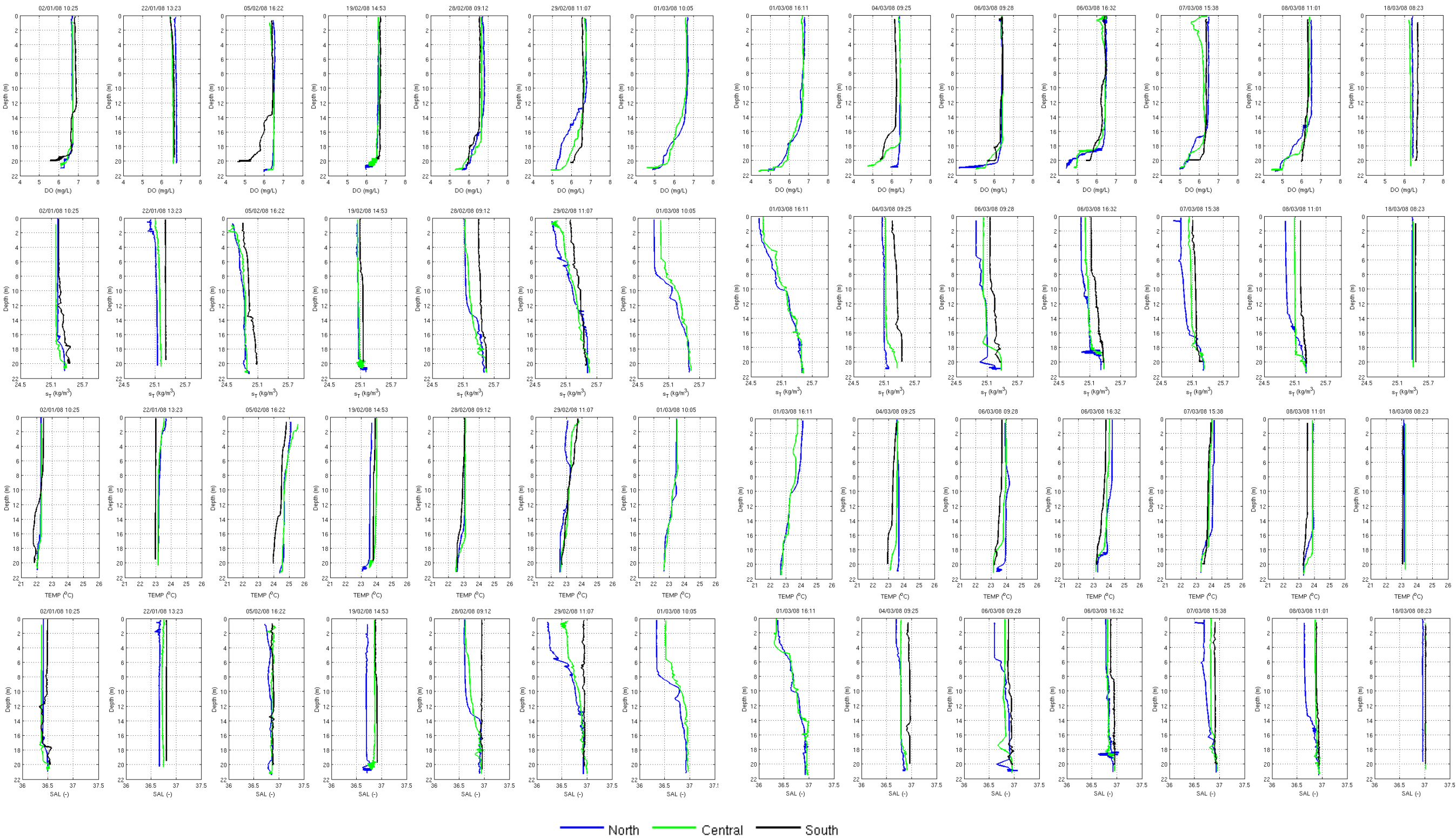


Figure 2-12 Dissolved oxygen, density, temperature and salinity measurements in Cockburn Sound

Site characterisation

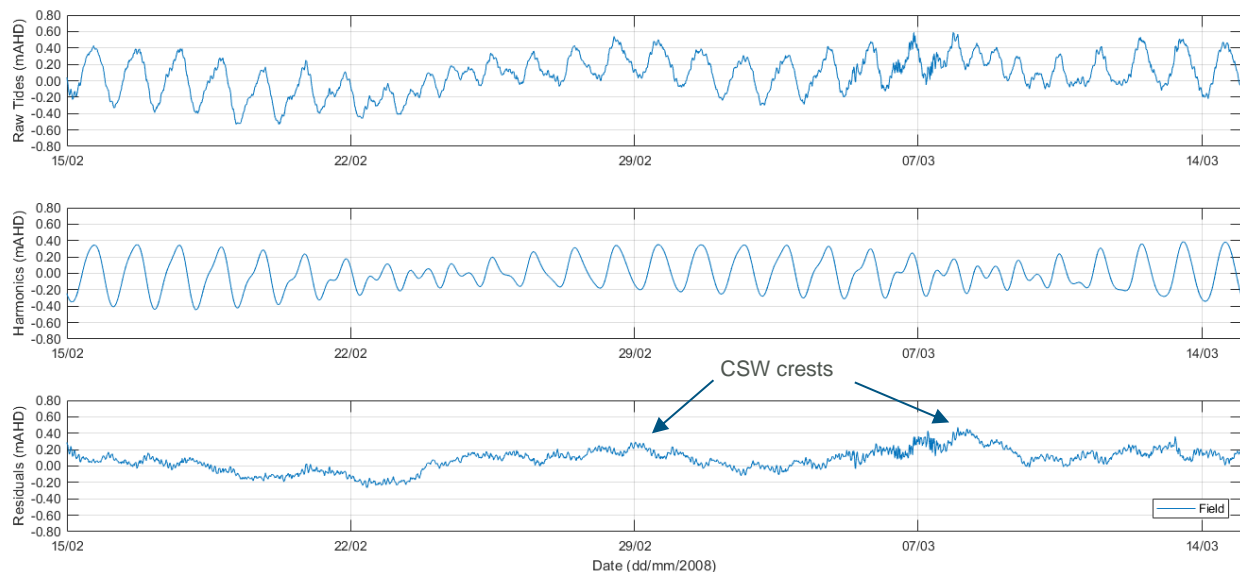


Figure 2-13 Tidal records at Mangles Bay from 15 February to 15 March 2008. Upper panel: Raw tidal record. Middle panel: harmonic components. Lower panel: residual water levels.

2.3.1 Low DO events

Following commissioning of the PSDP, a marine monitoring and management program (MMMP) was established by the Water Corporation in conjunction with the Office of the Environmental Protection Authority (OEPA) to ensure the PSDP brine discharge did not adversely impact the receiving environment. The key aspects of the MMMP consisted of real time monitoring of temperature, salinity, and dissolved oxygen (including near bed DO) and, during low dissolved oxygen events, manual plume tracking monitoring and an interim management response (Water Corporation 2013).

According to the Ministerial Condition 832 (OEPA 2010), a low dissolved oxygen event was defined as:

“... declines in dissolved oxygen of bottom waters, defined as less than or equal to 0.5 metres above the seabed, to 60% saturation (24 hour running median) or less in the high and/or moderate protection areas of Cockburn Sound as defined by the SEP”.

The MMMP was in place over the course of three years (2010 to 2013), a period over which the trigger for a management response occurred three times (February and May 2011, and April 2013 - Figure 2-14 and Figure 2-15). In particular, these events occurred between the end of summer and early autumn, and could be associated with low wind speeds, commonly below 5 m/s (Figure 2-15). As described above, this is the period over which stratification develops in Cockburn Sound as a result of the interplay between low wind speeds, density differences between the Sound and the adjacent oceanic waters, as well as the occurrence of CSWs. In 2011, the initial DO decline broadly coincided with the occurrence of TC Carlos and in 2013, the low DO events coincided with the occurrence of TC Victoria, therefore allowing for the possibility that CSWs may have played a role in local oxygen dynamics.

Site characterisation

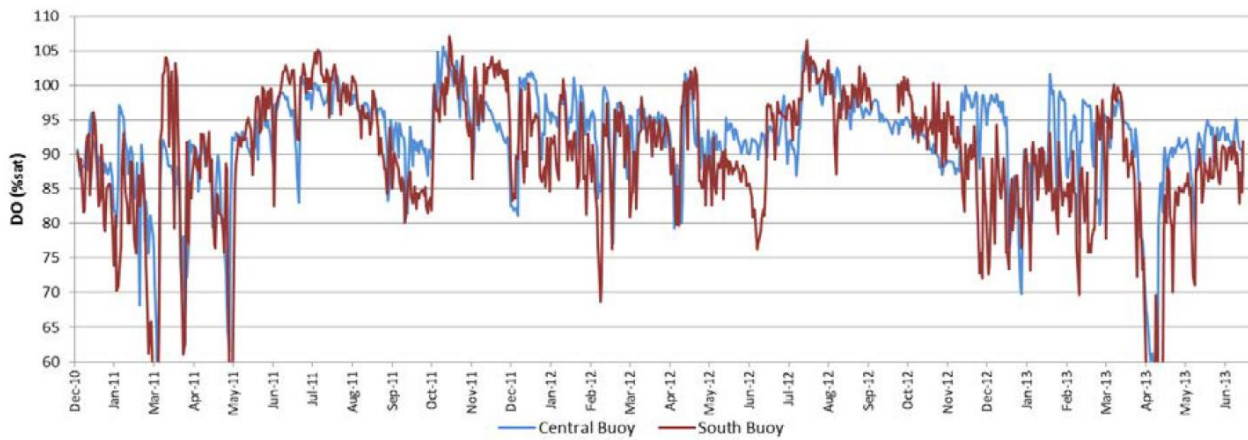


Figure 2-14 Continuous DO Monitoring conducted by the Water Corporation as part of the MMMP (Water Corporation 2013)

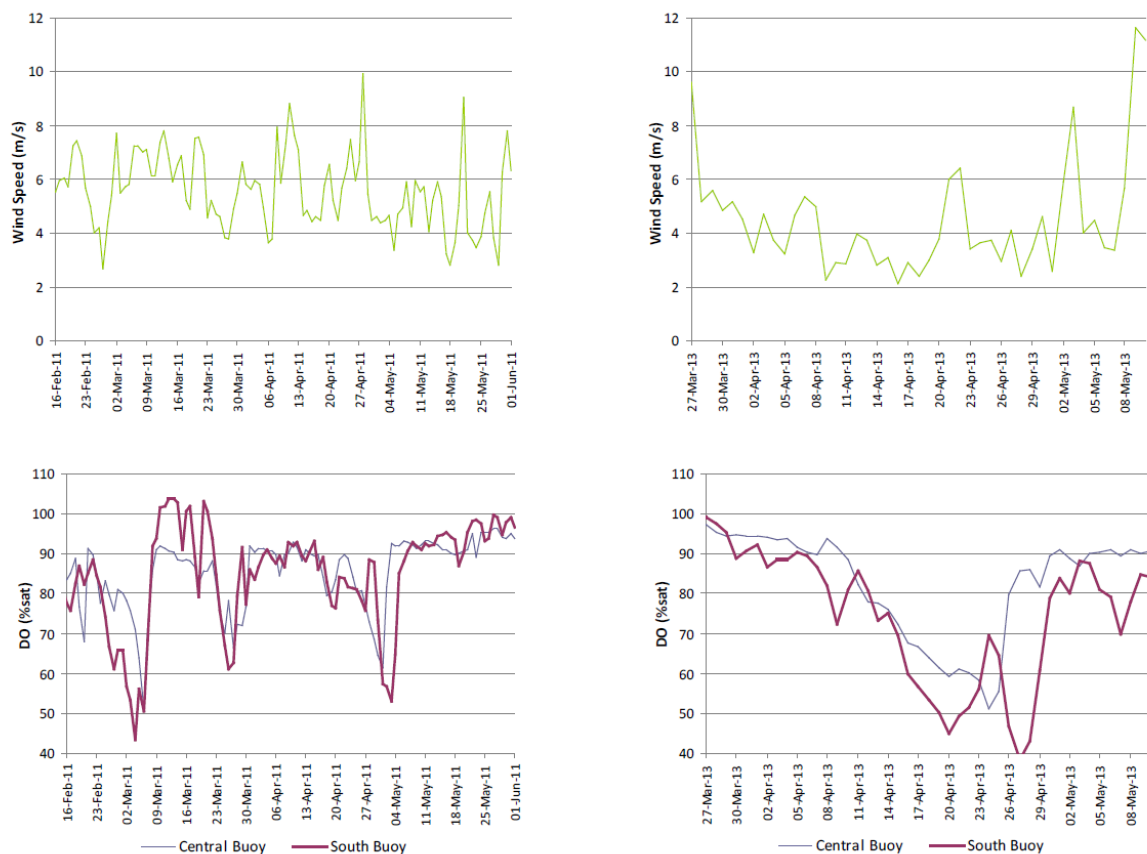


Figure 2-15 Wind speed and DO saturation during the low DO events of 2011 and 2013 (Water Corporation 2013)

Site characterisation

Data collected in April 2013 as part of the manual plume tracking monitoring under the MMMP illustrates the onset of a low DO event. Several concentrically distributed vertical profiles (including temperature, salinity, and DO) were collected over the event duration both in the deeper portion of Cockburn Sound (South and Central Buoys) in the transition between the Calista Channel to the deep basin of the Sound (Figure 2-16).

The DO, density, temperature and salinity data at Central and South Buoy are presented in Figure 2-17. Similar to the summer 2008 data, the development of low DO concentrations near the seabed followed the development of density stratification, generally associated with a less saline (but sometimes warmer) structure in the surface layer. However, and despite the lower temperatures in comparison to summer 2008 (thus associated higher DO saturation, Figure 2-12), the 2013 DO concentrations at depth were lower, and nearing 3 mg/L in some instances (Figure 2-17). Also, the DO concentrations were lower at South Buoy in comparison to the Central Buoy.

From the above, a picture emerges of how DO might be depressed at depth in autumn. Oxygen transfer via surface re-aeration is reduced as the wind intensity diminishes. At the same time, the density differences between the Sound and adjacent waters under the action of CSWs combine to strengthen vertical stratification of the water column, which in turn limits vertical mixing and transfer of DO to lower portions of the water column. As wind transfer is reduced and vertical stratification sets in, DO demand, particularly in the sediment, cannot be met by oxygen transfer at the surface, so DO concentrations become progressively lower until a meteorological and/or other event is sufficiently energetic so as to drive full water column mixing and therefore reaeration. For example, D'Adamo (2002) showed that, for full water column mixing in autumn, wind action alone is generally insufficient and penetrative convection from surface cooling is needed to provide the additional energy required to destratify the water column. For typical stratification strengths in autumn, a wind of 7.5 m/s combined with a surface heat loss of 300 W/m² requires approximately 13 hours to mix the entire water column (D'Adamo 2002).

Whilst low DO concentrations were observed in the deep basin of the Sound (Figure 2-17), low DO concentrations did not occur (at least not to the same extent) at the Calista Channel entry point (i.e. points R2, S2, S3, and A4 to A14 in Figure 2-16), and DO concentrations progressively decreased towards the deep basin, and particularly in the direction of the South Buoy station (Figure 2-18). These data therefore provided an indication that the depression in DO concentrations were likely being driven by large scale natural processes rather than stratification influenced by the PSDP discharge. As a result, and also confirmed by external peer review (GHD 2013), Water Corporation (2013) concluded the low DO event was unrelated to the PSDP discharge, but the result of the operation of other natural processes within Cockburn Sound.

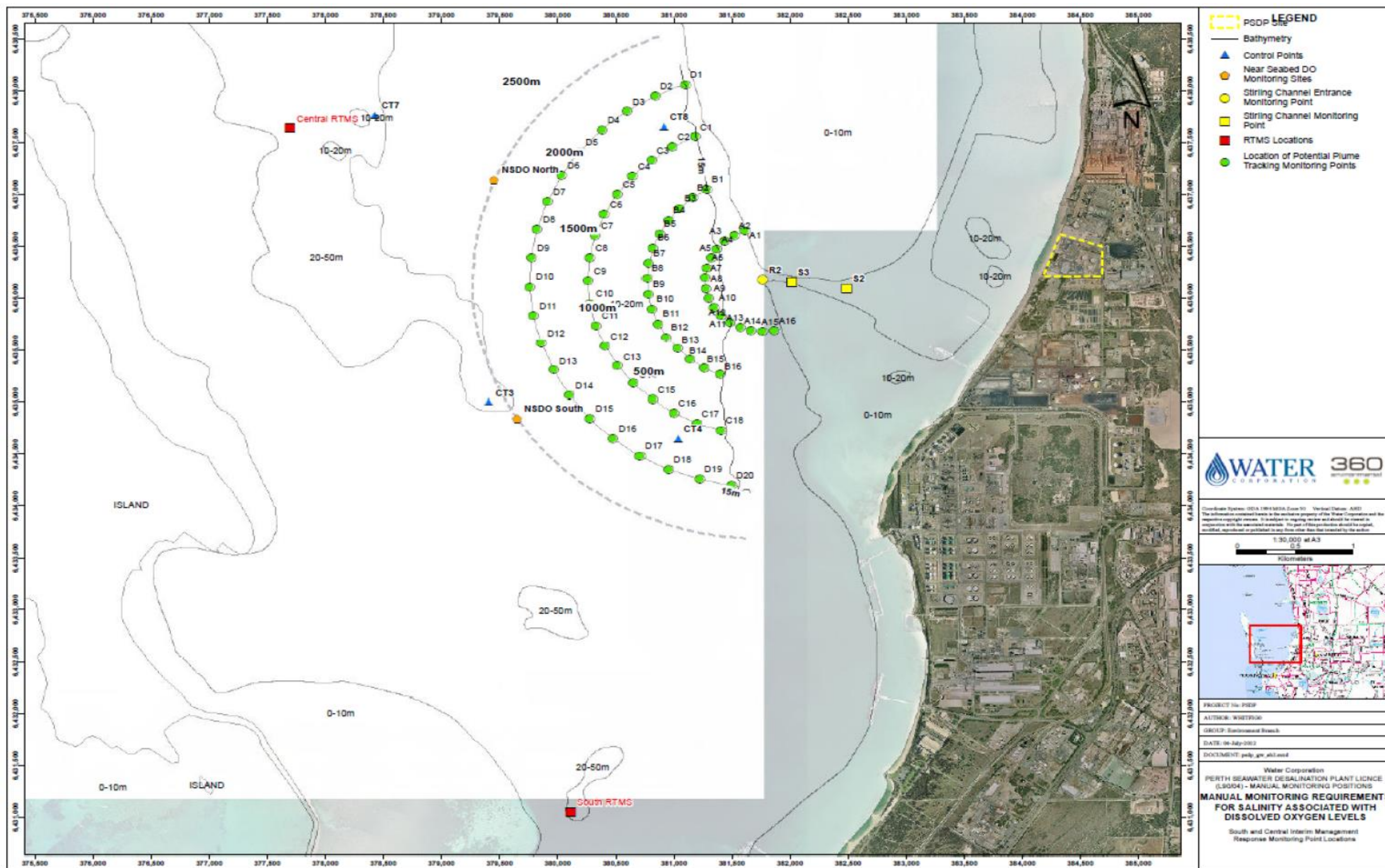


Figure 2-16 Locations at which profile data were sampled as part of the MMMP in April 2013 (from Water Corporation 2013)

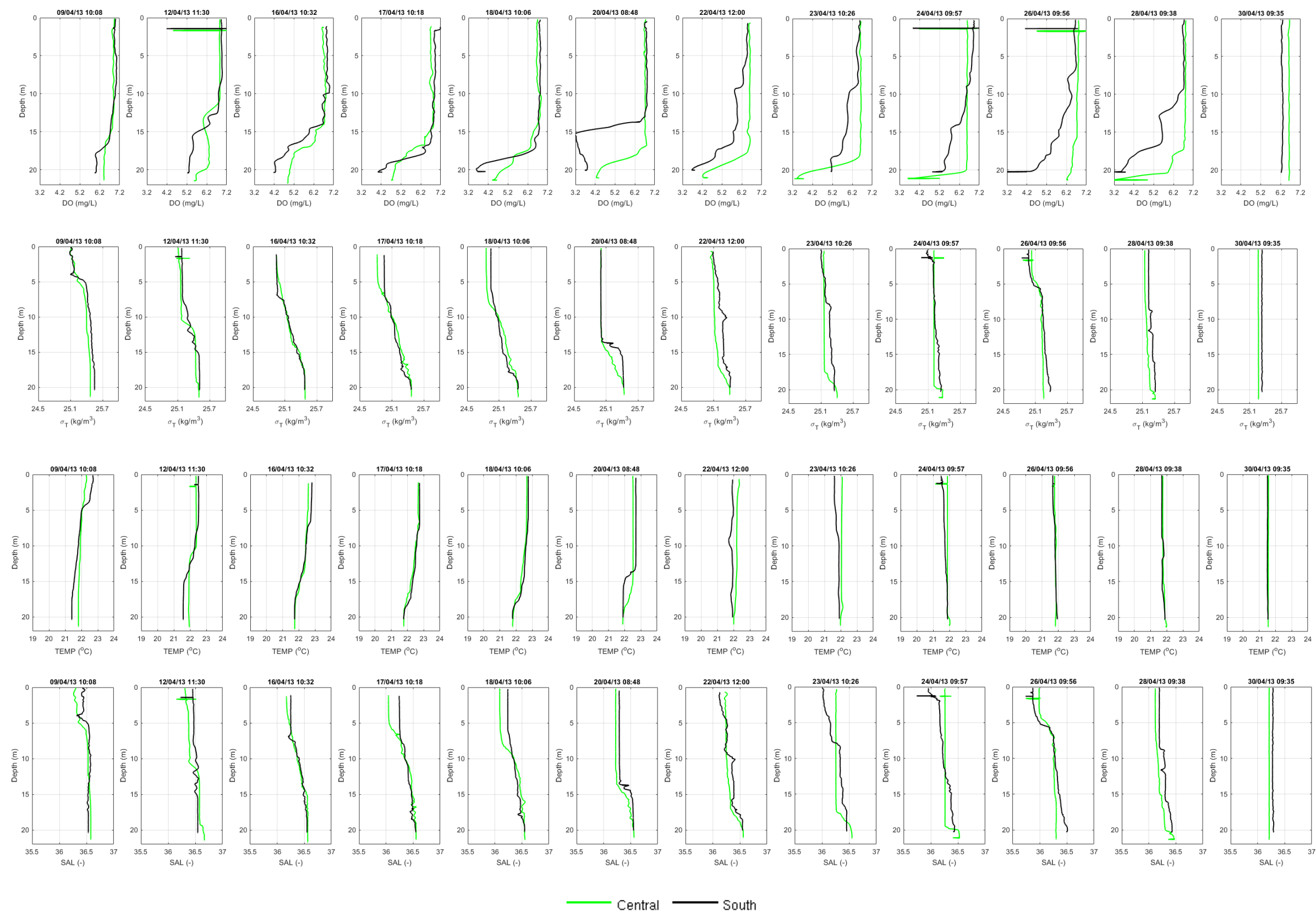


Figure 2-17 Dissolved oxygen, density, temperature and salinity measurements in Cockburn Sound in April 2013

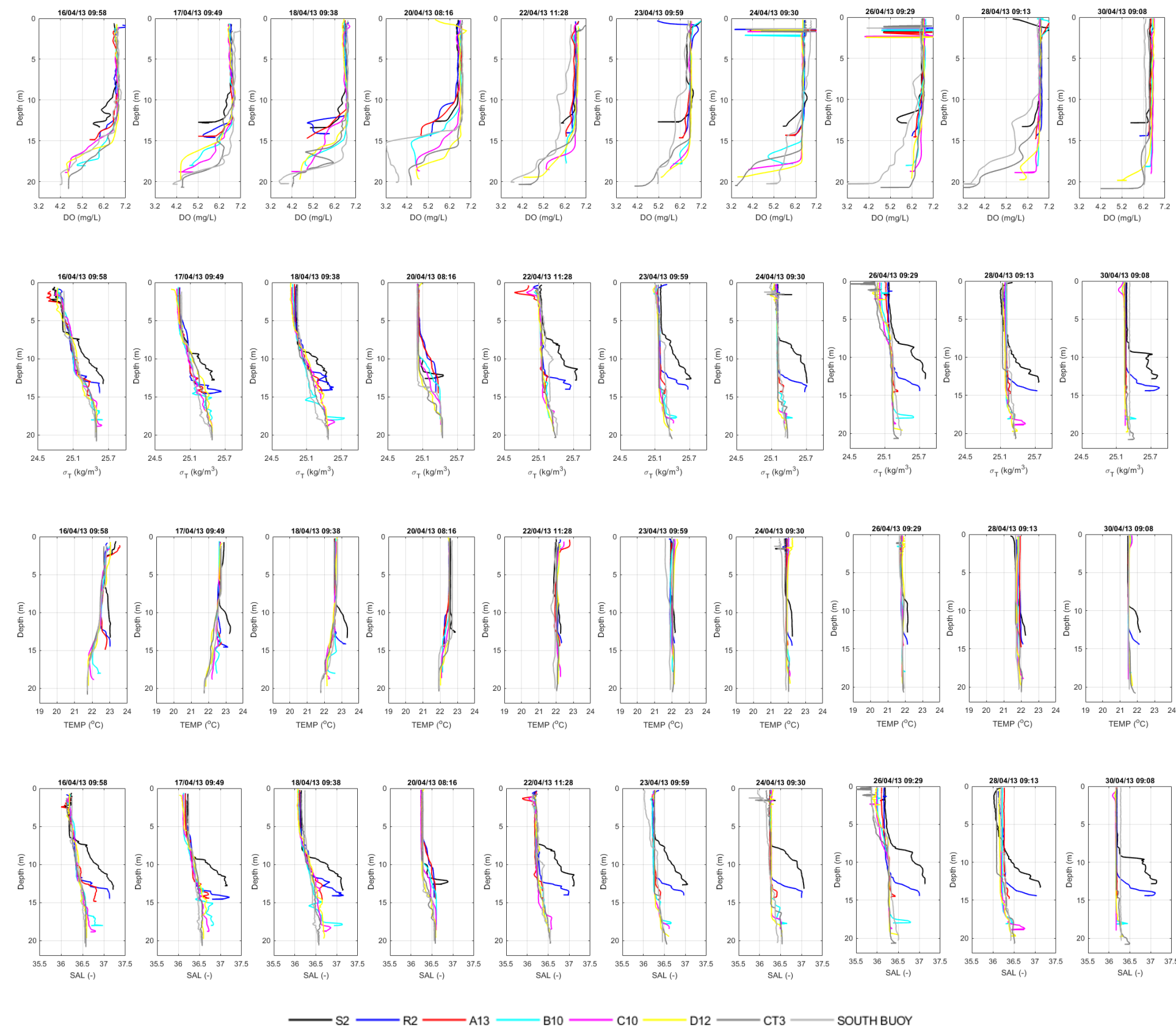


Figure 2-18 Dissolved oxygen, density, temperature and salinity measurements near Stirling channel entry in Cockburn Sound in April 2013. South Buoy profiles are also plotted for reference.

2.4 PSDP discharge characteristics

The existing desalination plant has a nominal production capacity of 45 GL/year, which requires the extraction of approximately 100 GL/year of seawater (assuming 45% recovery rate). Approximately 55 GL/year of high-salinity brine is returned to the coastal waters as part of the water treatment process. Other waste streams are also combined with the PSDP brine prior to discharge from time to time.

The effluent is discharged through an outfall located approximately 350 metres from shore at between approximately 9.4 m and 10.2 m (mAHD) as presented in Figure 2-19. The outfall manifold is aligned at 282.5° bearing and consists of a buried 1.65 m diameter pipeline, which bifurcates twice (double tee) into 1.20 m pipes (Figure 2-19). These pipes deliver the brine flows to a diffuser of approximately 163 m extension with forty 13 cm diameter ports (Figure 2-20). All ports are elevated 1.0 m from the seabed and point into a general northeast direction, which is approximately parallel with the shoreline. The ports are inclined to an angle of 60° to the vertical.

Flows to the outfall consist of the following sources (all nominal):

- Brine outflow with a contribution of 2.26 m³/s;
- Thickener flow with contribution of 0.070 m³/s;
- Dual media filter rinse with a contribution of 0.065 m³/s;
- Heat exchange flow with a contribution of 0.033 m³/s; and
- Backwater wash flow with a contribution of 0.084 m³/s.

The nominal intake flow rate is 4.23 m³/s. Assuming an ambient salinity of 36.5, the discharge salinity is approximately 61.4 (noting that salinity has no units).



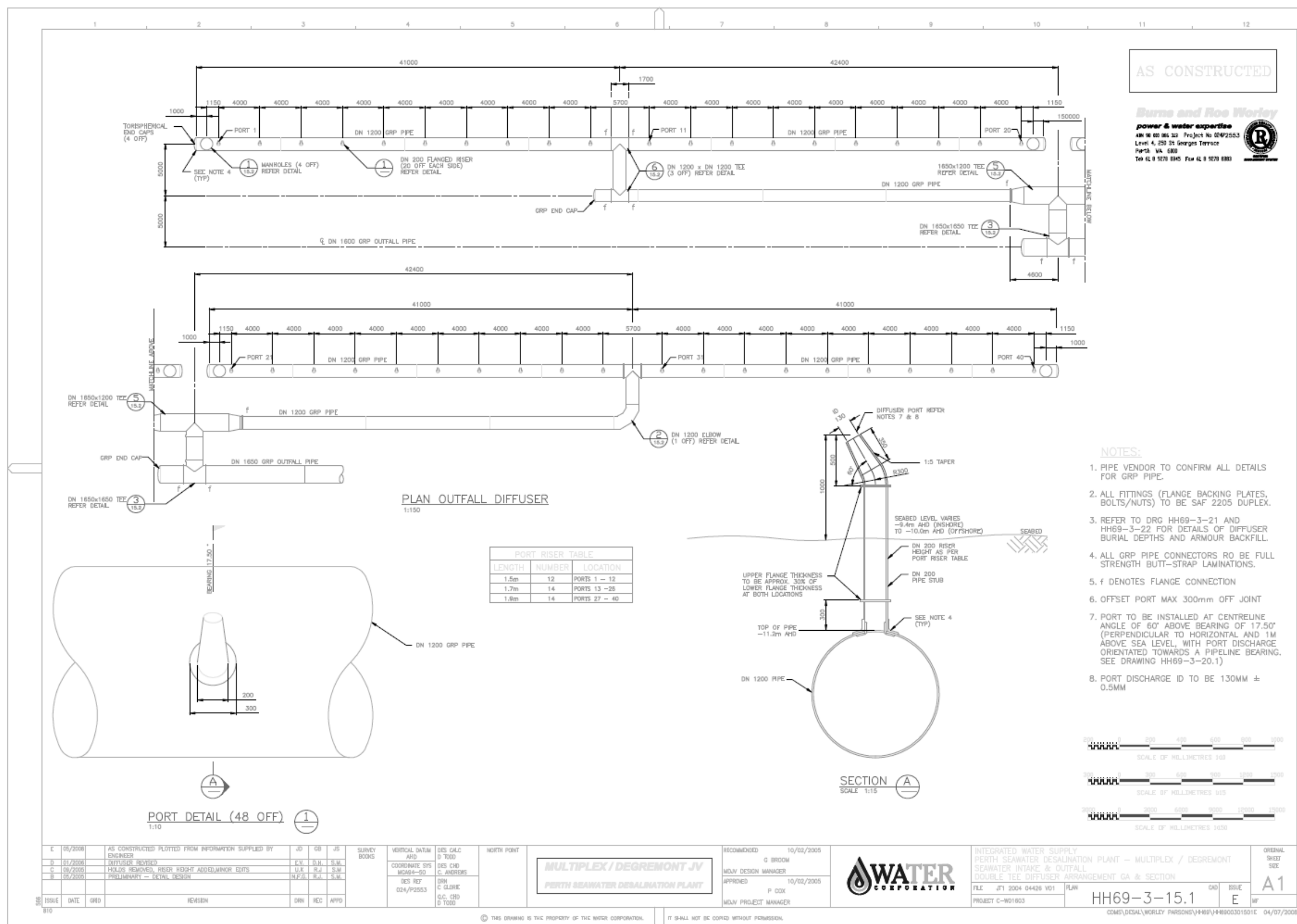


Figure 2-20 Seawater intake & outfall – double tee diffuser arrangement GA & section